Towards Prospective Disaster Risk Management: Mapping Multi-hazard Urban Risk Dynamics Driven by Evolving Exposure and Vulnerability via Earth Observation

Joshua Dimasaka[a,b,c,*], Fouad Bendimerad[c], Renan Ma. Tanhueco[c,d], Christian Geiß[e,f] and Emily So[a,b]

[a]Department of Architecture, University of Cambridge, United Kingdom
[b]Cambridge University center for Risk in the Built Environment, United Kingdom
[c]Earthquakes and Megacities Initiative, Philippines
[d]Department of Civil Engineering, De La Salle University, Philippines
[e]Earth Observation Center, German Aerospace Center, Germany
[f]Institute of Geography, University of Bonn, Germany

ARTICLE INFO

Keywords:
spatiotemporal
multi-hazard
prospective risk
exposure
physical vulnerability
neighborhood
barangay
city

ABSTRACT

As local governments increasingly adopt geospatial Climate and Disaster Risk Assessment (CDRA) to inform prospective public policy, the reliability of existing static risk intelligence is challenged by the continuous evolution of building exposure, population distribution, and physical vulnerability. Recent multi-temporal datasets of the built environment, derived from Earth Observation, have enabled comprehensive regional exposure-hazard analyses, yet their intersection with physical vulnerability remains underexplored. This study evaluates multi-hazard urban risk dynamics under the compounding effects of earthquake and flood in Quezon City, Philippines, using high-resolution multi-temporal building height data and Sentinel-2 imagery for projecting exposure and vulnerability through probabilistic graph deep learning. To extend the current CDRA and static Barangay Vulnerability Index (BVI), we present annual development profiles in terms of compound annual growth rate (CAGR) of its existing risk metrics spanning 2016–2030, covering building exposure, physical vulnerability, and earthquake-flood risk indicators. Against a baseline of 41,935 injuries for hospitalization and 12,494 fatalities, our projections indicate annual increases of up to +298 injuries and +85 fatalities, with 24 barangays identified with high earthquake- and high flood-induced displacement growth. Variability in growth trajectories across 142 barangays reflects the documented northward expansion of urban development, contrasting with redevelopment-driven patterns in the highly urbanized southern districts. Overall, our findings highlight spatially uneven trajectories of multi-hazard risk, underscoring the need for participatory validation with planners and policymakers to translate these spatiotemporal risk profiles into representations that are accessible, actionable, and impactful for prospective disaster risk management in cities undergoing rapid urbanization.

1. Introduction

In the increasing adoption of digital mapping technologies in many local governments, the geospatial knowledge on Climate and Disaster Risk Assessment (CDRA) has become the scientific backbone that directly underpins many critical public policy instruments (Amaratunga et al., 2019; Costa et al., 2024), such as comprehensive land use plans (Lagmay et al., 2024), emergency management (Freire et al., 2013), healthcare resource management (Hou et al., 2023), risk transfer financing mechanisms (Cabi et al., 2021), and recovery aid allocation (Loos et al., 2020). However, as the scale of climatic hazards intensifies and cascades, coupled with the accelerating urbanization, such risk intelligence is becoming outdated. This limitation primarily stems from the static representation of physical asset exposure through fixed building stock inventories, which often contain varying levels of uncertainty (Schorlemmer et al., 2026; Huyck et al., 2022).

Amidst the institutional barriers and challenges in local capacity (Malalgoda et al., 2016), this raises a critical question on how frequently local governments can update, fund, and re-conduct their geospatial risk assessments to ensure that their public policies remain relevant to the increasing exposure of the growing vulnerable population. As local governments continuously revise public policies through fiscal appropriations, the reliability of disaggregated risk information becomes critical to the sustainable and equitable reduction and management of climate and disaster risk at the community level. Beyond improving the accuracy of exposure information with the most up-to-date characterization, tracking the trajectory of historical changes in geospatial risk information can pinpoint areas that require targeted, localized solutions for prospective disaster risk management at scale.

The United Nations Office for Disaster Risk Reduction (UNDRR) (2017) defines prospective disaster risk management (PDRM) as a set of activities that "address and seek to avoid the development of new or increased

*Corresponding author
jtd33@cam.ac.uk; dimasakajoshua@gmail.com (J. Dimasaka)
ORCID(s): 0000-0001-9618-9431 (J. Dimasaka); 0009-0008-9915-3942 (F. Bendimerad); 0000-0001-5792-9871 (R.Ma. Tanhueco); 0000-0002-7961-8553 (C. Geiß); 0000-0002-2460-0452 (E. So)

disaster risks." In their recent Global Assessment Report on Disaster Risk Reduction (GAR) (UNDRR, 2025a) and Strategic Framework 2026-2030 (UNDRR, 2025b), the future-oriented decision-making aspect of PDRM can involve the use of tools such as probabilistic hazard models with metrics like average annual loss (AAL) and probable maximal loss (PML) or through the integration of demographic and urban growth projections for enhancing exposure and vulnerability data. While the use of AAL and PML from probabilistic hazard models is suitable for pricing catastrophe insurance policies for individual housing market or shared economy-wide entities like risk pools among cities and countries (Gignac-Eddy et al., 2020), the technical and fiscal capacity of many local governments at the scale of neighborhoods are, however, more appropriately positioned to public policies on emergency preparedness and post-disaster recovery, which rather rely on the deterministic- or scenario-based hazard maps (McGuire, 2001). Several studies have also shown that local governments with significant social ties to their communities and local knowledge play a key role on the frontlines of disaster risk management (Basu et al., 2013).

In this context, how projections of demography and urban growth influence the spatiotemporal distribution of exposure and vulnerability can provide the basis for developing local PDRM plans. Several studies have shown how this can inform (1) urban planning policies in the cities of Hanoi (Vietnam), Nagoya (Japan), Shanghai (China), and Hartford (United States) (Pham et al., 2011); (2) future multi-hazard risk management in Vancouver (Canada) (Chang et al., 2019); and (3) people-centered decision-making for post-disaster financial assistance programs and building code compliance in Istanbul (Türkiye), Nablus (Palestine), Chattogram (Bangladesh), Cox's Bazaar (Bangladesh), Nairobi (Kenya), Nakuru (Kenya), Quito (Ecuador), Kokhana (Nepal), Rapti (Nepal) and Darussalam (Tanzania) (Cremen et al., 2022, 2023, 2026). However, as a demonstrated case study in this work, while the Philippine government mandates the development of a Comprehensive Land Use Plan (CLUP) from which CDRA becomes vital (HLURB, 2013), current CDRA in practice (EMI, 2022) remains limited to fixed building stock inventories and other exposure indicators such as population, although climate projections are integrated (HLURB, 2015). Limited to hazard-based alone, this shortcoming is primarily driven by the lack of available and validated temporal data for fine-grained community-level projections, as well as by the inherently expensive data collection and monitoring requirements. Consequently, this reflects a policy gap, yet an ample opportunity in mainstreaming PDRM across all elements of climate and disaster risk.

The increasing availability of global multi-temporal datasets from Earth Observation and volunteered geographic information systems (Woods et al., 2025; Sirko et al., 2021, 2023; Glazer et al., 2025; Pesaresi et al., 2024; Marconcini et al., 2021) has enabled a growing body of research on quantifying evolving exposure and vulnerability patterns under the compounding and cascading effects of multiple hazards. Drawing on these datasets, recent studies have investigated the spatiotemporal intersections of built-up expansion, population growth, and hazard intensification across a range of contexts and scales. Stalhandske et al. (2025) documented a 69% global increase in per capita exposure to three or more hazards, including heatwaves, droughts, wildfires, extreme precipitation, river floods, and tropical cyclones, between 2003 and 2021 using the WorldPop population dataset at 0.25-degree resolution. Wang et al. (2026) demonstrated increasing exposure of human settlements to landslide susceptibility elevated by intensified rainfall patterns from 2000 to 2025 using Global Human Settlement Layer products at 0.1-degree resolution. Rentschler et al. (2023) revealed rapid global urbanization within flood zones since 1985 using DLR World Settlement Footprint data at 30-m resolution. At the city scale, Xia et al. (2026) identified three distinct developmental stages in the dryland expansion of Windhoek, Namibia, through the relationship between informal settlement growth and land surface temperature using the Google Open Buildings 2.5D Temporal dataset and Landsat imagery at 50-cm and 30-m resolution, respectively, while Lee and Kim (2026) analyzed daytime and nighttime population exposure under compounding earthquake-flood scenarios (Quigley and Duffy, 2020) in Seoul, South Korea, at 250-m resolution. Despite the valuable insights into multi-hazard urbanization dynamics, their focus on the spatiotemporal intersection of exposure and hazard alone does not yet translate into a risk-informed understanding, without accounting for physical vulnerability.

Our Contribution. Our work demonstrates multi-hazard urban risk dynamics driven by both evolving exposure and vulnerability, derived from Earth observation data, through probabilistic graph deep learning (Dimasaka et al., 2026b), using the case study of Quezon City (Philippines). At the neighborhood-to-city scale, we provide a significant extension to previous regional risk assessment of Quezon City (EMI, 2022; Dimasaka, 2022; Allen et al., 2014), a city with about 3 million population in 142 administering neighborhoods (hereafter, *barangay* or *brgy*) exposed to both magnitude-7.2 West Valley Fault earthquake scenario and recurring flooding events comparable to RCP8.5 100-year return period. Complementing the absolute measures of earthquake and flood risk, our work generates maps of annual development profiles of building exposure and population, physical vulnerability in terms of building material, earthquake risk by building damage state and casualty, and multi-hazard displacement, thereby providing the local government of Quezon City with relevant risk-informed insights for developing their local forward-looking PDRM plans. Our integration of the Google Open Buildings 2.5D Temporal dataset also presents improvements in the existing static geospatial exposure database.

The remainder of this chapter is organized as follows: Section 2 describes the geography and risk profile of Quezon City, including the datasets across the three elements of risk: multi-temporal high-resolution building exposure, prior physical vulnerability, and multi-hazard scenarios. Section 3 provides an overview of the implementation of probabilistic graph deep learning, a data-driven model of exposure and vulnerability, and then presents the assessment of earthquake and flood risk. Section 4 discusses the derived maps of annual development profiles, followed by the reported improvements on the existing exposure database and benchmarking with the most recent CDRA of Quezon City. Section 5 enumerates various methodological limitations as opportunities that can be further addressed in future work.

2. Materials

2.1. Study Area: Quezon City, Philippines

With a land mass of about 161 km^2, Quezon City in the northeast portion of Metro Manila has the largest population of over 2.9 million (as of 2015) among all 33 highly urbanized cities in the Philippines, occupying over one-fourth of the size of the metropolitan (QCPDO, 2022). The city comprises six districts (numbered 1-6) with 37, 5, 37, 38, 14, and 11 barangays, respectively, as shown in Figure 1, Figure 2, and Figure 3. Over the years, the city has urbanized with about 30% residential with a ribbon-type commercial development concentrated around major transportation networks. Despite the growing demography of predominantly young at a median age of 27, the QCPDO (2022) further reported that, in 2022, about 209,350 families still lived in informal settlements, and, in 2021, the poverty incidence rate (among population) is at 3.0%, which is equivalent to 94,134 residents with insufficient income for minimum basic needs. This critical background information is important in the context of our work that examines the growth in multi-hazard displacement, exacerbating these existing socio-economic conditions of the city.

2.2. Multi-temporal High-Res Building Exposure

The exposure dataset of Quezon City has undergone multiple refinements over two decades, evolving from the foundational Metro Manila Earthquake Impact Reduction Study (MMEIRS) in 2002 to 2004 (JICA et al., 2004). This improved in the 2006 Air Quality Study by the Metropolitan Manila Development Authority (MMDA) and subsequently by the 2014 Greater Metro Manila Area Risk Analysis Project (GMMA-RAP), the first megacity multi-hazard risk assessment to integrate time-series Landsat multi-spectral and aerial imagery, digital elevation and surface models at 1-m resolution, 2010 census data on population and housing, and other remote sensing information (Bautista et al., 2014). Despite extensive field survey validation, Bautista et al. (2014) recognized several modeling challenges, including cloud corruption and lighting illumination artifacts in satellite imagery,

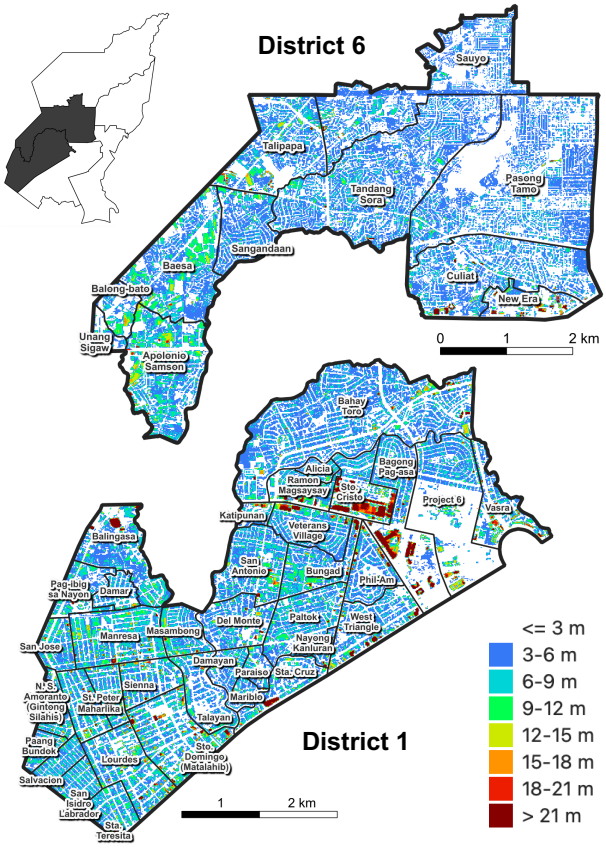

Figure 1: The administrative boundaries of barangays in Districts 1 and 6 (EMI, 2022) showing our derived 2020 building height data at 10-m resolution.

false negatives in building detection where rooftops were spectrally similar to vegetation or non-structural accessories such as covered walkways, uncertainty in inter-storey heights by occupancy type, incomplete census information for select barangays, and inherent model uncertainties from unsupervised land use classification. In 2013, Earthquakes and Megacities Initiative (EMI) centralized the first comprehensive geospatial exposure database at the city level using geographic information system tools (EMI, 2013), followed by a significant update in 2022 through manual digitization using the latest digital elevation and surface models and high-resolution orthoimagery at about 0.40-m resolution (EMI, 2022). These successive updates both reflect the growing interest in city exposure modeling in practice and the methodological challenges that motivate the probabilistic and data-driven approach adopted in this work.

Building on these developments, this work leverages the publicly available high-resolution 50-cm annual building height data from the Google Open Buildings 2.5D Temporal dataset (2016 to 2021), derived from Copernicus Sentinel-2 imagery through a super-resolution technique with a mean absolute error of 1.5 m and a coefficient of determination, R^2, of 0.91 (Sirko et al., 2023). Recognizing that building height data alone provides

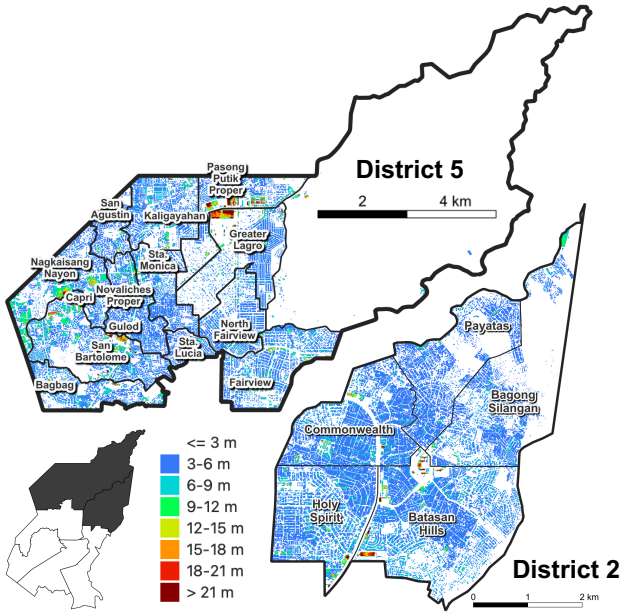

Figure 2: The administrative boundaries of barangays in Districts 2 and 5 (EMI, 2022) showing our derived 2020 building height data at 10-m resolution.

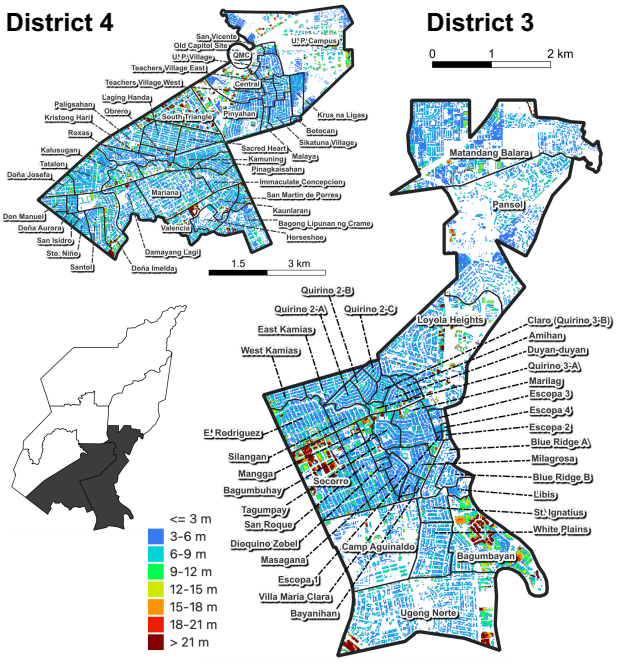

Figure 3: The administrative boundaries of barangays in Districts 3 and 4 (EMI, 2022) showing our derived 2020 building height data at 10-m resolution.

insufficient discriminative power for material typology classification to support the probabilistic graph deep learning, we incorporated additional physically interpretable covariates from Copernicus Sentinel-2 imagery, including multi-spectral bands and other derived spectral indices (Dimasaka et al., 2026b). Hence, we resampled these building height maps at 50-cm resolution into coarser 10-m

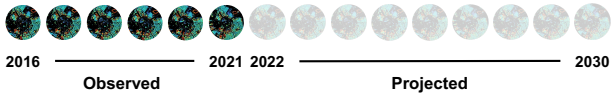

Figure 4: Evolving exposure patterns of building height from the Google Open Buildings 2.5D Temporal dataset (Sirko et al., 2023) where the periods 2016-2021 and 2022-2030 serve as observations and projections, respectively.

grids and expressed the building height ($\mathbf{E_{BH}}$) within each grid using the non-negative constraint (i.e., $\mathbf{E_{BH}} \geq 0$) of the lognormal probability distribution as:

$$\ln \mathbf{E_{BH}} \sim \mathcal{N}(\boldsymbol{\mu}, \boldsymbol{\Sigma}) \tag{1}$$

where $\boldsymbol{\mu}$ and $\boldsymbol{\Sigma}$ are the mean and variance of fine-grained building height values at 50-cm resolution within each 10-m grid. The resulting 2016-2021 maps serve as prior distributions for building heights, which are inputs to our graph-based deep neural network with parameters $\boldsymbol{\theta}$ that transform the prior parameters $(\boldsymbol{\mu}, \boldsymbol{\Sigma})$ into posterior estimates $(\boldsymbol{\mu}_\theta, \boldsymbol{\Sigma}_\theta)$, enabling projections for the period from 2022 to 2030, as shown in Figure 4. To illustrate, Figure 1, Figure 2, and Figure 3 show our derived 2020 building height data at 10-m resolution.

2.3. Prior Physical Vulnerability

The physical vulnerability of Quezon City's building stock, characterized herein as building material typology, has been refined across two successive exposure developments. In the 2014 GMMA-RAP, Bautista et al. (2014) addressed the absence of building-level material typology data by leveraging coarse-grained 2000 census surveys on roof material types, such as galvanized iron, tile, concrete, wood, and makeshift, and wall material types, such as concrete, wood, and makeshift. Bautista et al. (2014) expressed the composition of each building material typology as proportions of building counts and floor area per roof-wall combination within defined polygonal areas, as shown in Figure 5. The 2022 CDRA update adopted this representational detail while substantially enhancing its spatial precision through the integration of the latest digital elevation and surface models and high-resolution orthoimagery (EMI, 2022). While each roof-wall combination corresponds to a physical vulnerability typology label, such as **C1L** for low-rise reinforced concrete moment frames, that can be synchronized with fragility and vulnerability functions in standard risk assessment (Bautista et al., 2012; Tingatinga et al., 2019), the difficulty of one-to-one and one-to-many associations between roof-wall combinations and building material typologies remains a methodological challenge in ascertaining the true distribution of physical vulnerability. In other work, we addressed this difficulty using the combination of fuzzy mapping and deep learning-based spatial disaggregation using census as constraints to a clustering task (Dimasaka et al., 2026a), which is beyond the

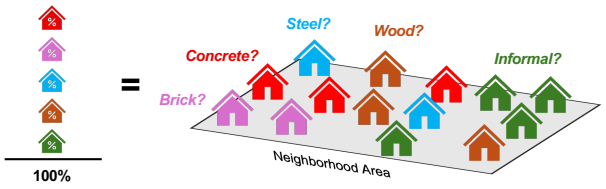

Figure 5: Schematic illustration of area-based approach.

scope of this study. Nonetheless, this area-based approach can serve as a prior distribution for our probabilistic categorical assumption, enabling deep learning-based Bayesian updating toward a finer-grained spatiotemporal distribution of physical vulnerability across Quezon City.

Following the formulation from the preceding section, we rasterized the building material typology from the 2022 exposure database at a 10-m grid resolution, expressing the physical vulnerability ($\mathbf{V}$) of each cell as a categorical random variable under a multinomial probability distribution as:

$$\mathbf{V} \sim \text{Mult}(\boldsymbol{p}^1, \ldots, \boldsymbol{p}^K) \tag{2}$$

where $\boldsymbol{p}^1, \ldots, \boldsymbol{p}^K$ are the compositional values of $\mathbf{K}$ building typologies summing to 1.0 within each 10-m grid. Unlike the multi-temporal building exposure, the prior for physical vulnerability is static and non-time-varying across the 2016 to 2021 period, reflecting an underexplored opportunity in large-scale monitoring of building typologies using Earth observation data. In the same way, our graph-based deep neural network with parameters $\boldsymbol{\theta}$ transforms the prior parameters $(\boldsymbol{p}^1, \ldots, \boldsymbol{p}^K)$ into posterior estimates $(\boldsymbol{p}^1_\theta, \ldots, \boldsymbol{p}^K_\theta)$, enabling temporal inference for the period from 2016 to 2030. Recognizing this current limitation brought about by the lack of temporal building typology data, this also presents an opportunity for future iteration for recalibration studies, when data becomes available. Such data can range from a new census of population and housing to emerging research innovations, including temporal disaggregation tools (Huber et al., 2026) and OpenBuildingMap (Schorlemmer et al., 2026; Oostwegel et al., 2025), which leverage the temporal evolution of OpenStreetMap data, a form of volunteered geographic information of building typology (Bennett, 2010).

We grouped these detailed typologies into broader material classification, as shown Table 1, and summarized their presence in each district and barangay in the supplementary file.

2.4. Multi-Hazard Scenarios

The compound effects of sequential hazards, wherein a large earthquake is followed by flooding or vice versa, are important in Quezon City, where existing human settlements reside within and around an earthquake fault line, alongside recurring hydrometeorological hazards. Scenarios such as a major earthquake during the typhoon season or an impending typhoon landfall during the aftermath of a large

Table 1
Building material classifications of detailed typologies.

Material	Symbol	Description
Wood	**W1W3**	Wooden light-frame (small)
	W2	Wooden light-frame (large)
	N	Makeshift or informal
Masonry	**CHBMWS**	Concrete hollow block
	URA	Unreinforced adobe walls
	URM	Unreinforced masonry walls
	RM2	Reinforced masonry walls
Concrete	**CWS**	Concrete with steel
	C1	Reinforced concrete frame
	C2	Reinforced concrete shear wall
	C4	Concrete shear walls & frames
	PC2	Precast concrete frames
Steel	**S1**	Steel moment frames
	S2	Steel braced frames
	S3	Steel light frames

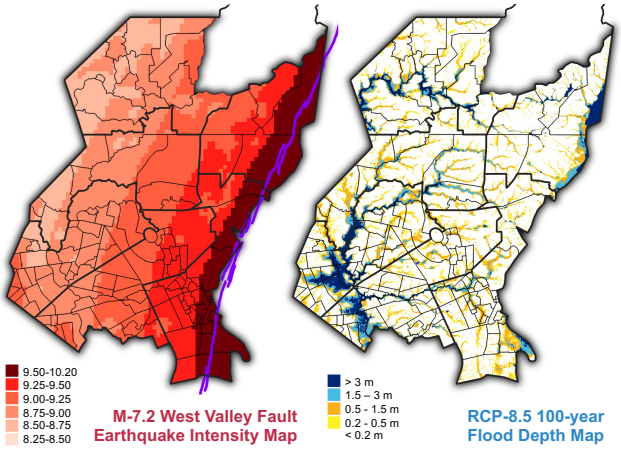

Figure 6: Multi-hazard scenarios: earthquake intensity map at 175-m scale (*left*) and flood depth map at 10-m scale (*right*) (EMI, 2022; QCDRRMO and UPRI-NOAH, 2022).

earthquake could dramatically exacerbate risks to affected communities. To explore this compound risk scenario, we considered the earthquake scenario of a magnitude-7.2 along the West Valley Fault in combination with a flooding simulation under the RCP8.5 with rainfall at a 100-year return period (EMI, 2022). As shown in Figure 6, we adopted the hazard maps from the 2022 CDRA of EMI (2022) to have a consistent comparison across risk metrics.

2.4.1. M-7.2 West Valley Fault Earthquake Intensity

Described as the "Big One" in public discourse and estimated as the maximum size from the MMEIRS project (JICA et al., 2004), the magnitude-7.2 earthquake scenario in the West Valley Fault is reportedly to have a return period between 400 and 600 years with an uncertainty range of 100-400 years, based on the paleoseismic studies by Nelson et al. (2000). Depending on the distance from

Table 2
Modified Mercalli Intensity Scale (Wood and Neumann, 1931).

MMI	Description
8	"Damage **slight** in specially designed structures; **considerable** in ordinary substantial buildings with partial collapse; **great** in poorly built structures. Panel walls thrown out of frame structures. Fall of chimneys, factory stacks, columns, monuments, and walls. Heavy furniture overturned. Sand and mud ejected in small amounts. Changes in well water. Disturbed persons driving motor cars."
9	"Damage **considerable** in specially designed structures; well-designed frame structures thrown out of plumb; **great** in substantial buildings, with partial collapse. Buildings shifted off foundations. Ground cracked conspicuously. Underground pipes broken."
10	"Some well-built wooden structures **destroyed**; most masonry and frame structures **destroyed** with foundations; ground badly cracked. Rails bent. Landslides **considerable** from riverbanks and steep slopes. Shifted sand and mud. Water splashed (slopped) over banks."

the fault rupture and soil characteristics through which the earthquake propagates, Figure 6 (*left*) maps the Modified Mercalli Intensity (MMI) (Wood and Neumann, 1931) (see Table 2 for descriptions) based on its empirical relationship with peak ground acceleration calculated from ground motion prediction models. EMI (2022) reports earthquake intensity in terms of MMI to ensure comparability with previous studies (MMEIRS and GMMA-RAP) and to support its interpretation and application by government practitioners who are more familiar with intensity-based scales than with engineering measures such as peak ground acceleration or spectral response values.

2.4.2. RCP8.5 100-year Flood Depth Map

As established in the Quezon City Drainage Master Plan (QCDRRMO and UPRI-NOAH, 2022), we used the flood depth map under the scenario of Representative Concentration Pathway (RCP) 8.5 (2020-2039) with rainfall at a 100-year return period, as shown in Figure 6 (*right*). The RCP8.5 scenario represents an upper-bound, business-as-usual trajectory (i.e., worst-case scenario) characterized by the highest projected greenhouse gas concentrations, compounded by the absence of climate mitigation measures and sustained high population growth (Riahi et al., 2011). This is also comparable in intensity to the observed inundation from severe tropical storm Ondoy, known internationally as Ketsana (EMI, 2022). The flood depth map is stratified into five increasing inundation levels: ($< 0.2m$) remain generally manageable; ($0.2 - 0.5m$) destabilize moving vehicles; ($0.5 - 1.5m$) pose casualty risks and disrupt light to medium vehicles; ($1.5 - 3.0m$) render households significantly non-functional; and ($> 3.0m$) displace residents to upper floor levels.

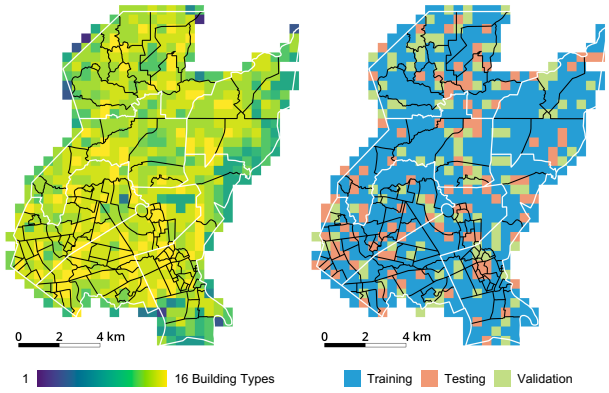

Figure 7: The varying number of building types (*left*) controls the splitting of dataset into training (70%), testing (15%), and validation (15%) sets (*right*).

3. Methods

3.1. Probabilistic Data-Driven Model

The probabilistic data-driven model, known as the Graph Variational State-Space Model provided in detail in Dimasaka et al. (2026b), trains four modules of graph-based deep neural network that approximates: (1) the relationship among the patterns of building height (exposure), input prior of material typology compositions (physical vulnerability), and other covariates from Copernicus Sentinel-2 imagery; and (2) the dynamics of posterior estimates for the lognormal and multinomial probability distributions of building exposure and physical vulnerability, respectively. Similar to Bayesian updating enhanced by probabilistic graph deep learning, it trains a set of parameters $\boldsymbol{\theta}$ for each posterior distribution by balancing new information across temporal periods against the prior information from the Google Open Buildings 2.5D Temporal dataset and the Quezon City's building stock with material typology characterization.

s

The graph-structured representation of building exposure and physical vulnerability incorporates neighborhood information from eight-directional adjacency[1] among 10-m pixels, establishing a learning propagation mechanism as the parameters $\boldsymbol{\theta}$ of a three-layer graph convolutional neural network[2] (Kipf and Welling, 2016) converge to an optimal solution. In each module of physical vulnerability, the variational autoencoder[3] learns a structured[4] latent[5] representation consistent

[1] eight directions: north, east, west, south, northeast, southeast, southwest, and northwest
[2] a type of graph-based deep neural network
[3] a deep learning solution that approximates the posterior estimates
[4] "structured" means the use of parameters of a probability distribution
[5] similar to the term"hidden" because the true compositions are not fully observed (or available)

Table 3
Inverse-step weighting approach.

		Inference														
		2016	2017	2018	2019	2020	2021	2022	2023	2024	2025	2026	2027	2028	2029	2030
Observations	2016	1	1/2	1/3	1/4	1/5	1/6	1/7	1/8	1/9	1/10	1/11	1/12	1/13	1/14	1/15
	2017		1	1/2	1/3	1/4	1/5	1/6	1/7	1/8	1/9	1/10	1/11	1/12	1/13	1/14
	2018			1	1/2	1/3	1/4	1/5	1/6	1/7	1/8	1/9	1/10	1/11	1/12	1/13
	2019				1	1/2	1/3	1/4	1/5	1/6	1/7	1/8	1/9	1/10	1/11	1/12
	2020					1	1/2	1/3	1/4	1/5	1/6	1/7	1/8	1/9	1/10	1/11
	2021						1	1/2	1/3	1/4	1/5	1/6	1/7	1/8	1/9	1/10

with the discrete categorical (i.e., multinomial) nature of physical vulnerability, extending the analytical Bayesian formulations of Pittore et al. (2020) and Porter et al. (2014) through the reparameterization trick of Jang et al. (2016). Model training optimizes the combined loss[6] comprising the reconstruction of decoded patterns, a Kullback-Leibler divergence loss[7] for the encoded posterior distributions of building exposure and physical vulnerability, and a semi-supervised cross-entropy loss (Kingma et al., 2014). As the number of available building material typologies varies across barangays (see supplementary file), we considered non-overlapping tiles of size 48x48 grid cells, split into training (70%), testing (15%), and validation (15%) sets, as shown in Figure 7.

For downstream inference, the trained model was applied to newly prepared overlapping tiles and aggregated pixel-wise to generate the final maps, producing six sets of probabilistic projections corresponding to each observed period from 2016 to 2021, each extending individually up to 2030. For example, the model conditioned on the 2016 observed measurement generates probabilistic projections for every period from 2017 to 2030, and similarly for each subsequent observed year. Because this produces multiple overlapping projections for any given future period, we applied a temporal weighting approach via $1/step$, wherein projections at closer temporal distance carry greater weight than those further from their conditioning observation, reflecting their comparatively higher reliability. To illustrate, a projection for 2017 conditioned on 2016 is just one step away and therefore weighted most heavily, while a projection for 2025 conditioned on 2016 is nine steps away and contributes proportionally less to the aggregated estimate. As shown in Table 3, this inverse-step weighting approach, when normalized column-wise, addresses the inherent imperfections of temporal prediction under limited historical observations, yielding a reliability-weighted composite map over the 2016-2030 horizon.

3.2. Earthquake and Flood Risk Assessment

Applying the same approach (Tingatinga et al., 2019; Allen et al., 2014) from the 2022 CDRA of EMI (2022)

[6] "loss" measures similarity against available observations

[7] a metric that compares the parameters of two probability distributions (i.e., prior vs posterior)

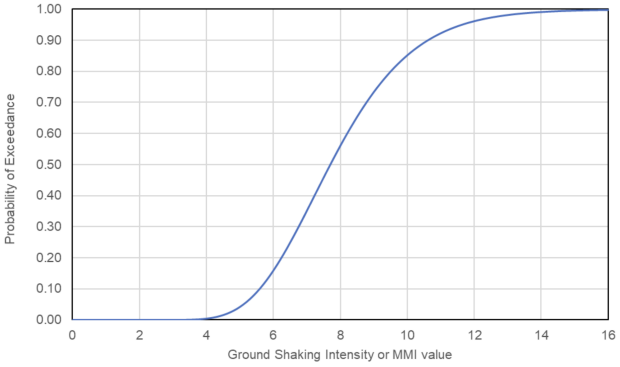

Figure 8: Example curve of lognormal distribution for the **Slight** damage state for a wooden light-frame building (adopted from (Dimasaka, 2022).

on the inferred annual posterior samples of building height (exposure) and material typology compositions (physical vulnerability) from 2016 to 2030, we calculated the distribution of earthquake-damaged floor area at varying states: **None**, **Slight**, **Moderate**, **Extensive**, and **Complete**, which is further classified into **Complete without Collapse** and **Complete with Collapse**.

The earthquake risk assessment follows the standard probabilistic approach (Baker et al., 2021; Cornell et al., 1968; FEMA, 2022) wherein each damage state assumes a lognormal probability distribution that is parameterised through median and standard deviation of ground shaking intensity. In symbols,

$$P(\mathrm{DS} \geq ds \mid IM) = \Phi\left(\frac{\ln(IM/IM_m)}{\beta}\right) \tag{3}$$

where Φ is the standard normal cumulative distribution function. Figure 6 (*left*) provides the input intensity (IM). The parameters, median (IM_m) and standard deviation (β), for each damage state (ds) by material typology for the local building stock are available from Tingatinga et al. (2019) and FEMA (2022). To illustrate, Figure 8 plots the probability of *exceeding* the **Slight** damage state for a wooden light-frame building and describes the physical interpretation of each damage state in Table 4.

We calculated the probabilities of *exceedance* for all damage states, and evaluated their differences to obtain the

Table 4
Physical interpretation of damage states for a wooden light-frame building FEMA (2022).

Damage State	Description
Slight	"Small plaster or gypsum-board cracks at corners of door and window openings and wall-ceiling intersections; small cracks in masonry chimneys and masonry veneer."
Moderate	"Large plaster or gypsum-board cracks at corners of door and window openings; small diagonal cracks across shear wall panels exhibited by small cracks in stucco and gypsum wall panels; large cracks in brick chimneys; toppling of tall masonry chimneys."
Extensive	"Large diagonal cracks across shear wall panels or large cracks at plywood joints; permanent lateral movement of floors and roof; toppling of most brick chimneys; cracks in foundations; splitting of wood sill plates and/or slippage of structure over foundations; partial collapse of "room-over-garage" or other "soft-story" configurations; small foundation cracks."
Complete	"Structure may have large permanent lateral displacement, may collapse, or be in imminent danger of collapse due to cripple wall failure or the failure of the lateral load-resisting system; some structures may slip and fall off the foundations; large foundation cracks."

probability of *being* in each damage state. For each grid cell, we multiply this probability of *being* in a particular damage state with the total floor area from our inferred posterior maps to estimate the corresponding damaged floor area.

Using the population rate per unit of floor area that is extrapolated and uniformly applied from various public statistics data (PSA, 2026b), we evaluated the corresponding casualties or injuries at increasing four severity levels, as shown in Table 5. In addition, we estimated the earthquake-induced displacement by using the population under the **Extensive** and **Complete** damage states. Similarly, the flood risk assessment deals with overlaying the map of buildings with one to two floor levels with the critical flood depth at 0.5 m, a threshold that triggers flood-induced displacement.

3.3. Derivation of Annual Development Profile

We generated maps of expected annual growth in built-up area, population, building material, earthquake risk, and multi-hazard human displacement using two measures: (1) average annual change in absolute values and (2) the compound annual growth rate (CAGR), expressed as:

Table 5
Injury classification scale (FEMA, 2022).

Severity	Description
Slight Injuries	"Injuries requiring basic medical aid that could be administered by paraprofessionals. These types of injuries would require bandages or observation. Some examples are a sprain, a severe cut requiring stitches, a minor burn (first-degree or second-degree on a small part of the body), or a bump on the head without loss of consciousness."
Serious Injuries	"Injuries requiring a greater degree of medical care and use of medical technology such as x-rays or surgery, but not expected to progress to a life-threatening status. Some examples are third-degree burns or second-degree burns over large parts of the body, a bump on the head that causes loss of consciousness, or fractured bone."
Life-threatening Injuries	"Injuries that pose an immediate life-threatening condition if not treated adequately and expeditiously. Some examples are uncontrolled bleeding, punctured organ, other internal injuries, spinal column injuries, or crush syndrome."
Fatalities	"Instantaneously killed or mortally injured."

$$\mathrm{CAGR} = \left(\frac{Y_{\mathrm{T}}}{Y_0}\right)^{\frac{1}{t_{\mathrm{T}}-t_0}} - 1 \tag{4}$$

where Y_0 and Y_{T} are the measurements at times t_0 and t_{T}, respectively. Based on the CAGR values, we stratified the 142 barangays into quintiles (approximately 28 barangays per group) and assigned them to five descriptive growth tiers: **Lowest**, **Lower-Mid**, **Median**, **Upper-Mid**, and **Highest**. We refer to the resulting ranked maps as *annual development profiles*, which characterize the annual growth patterns of barangays from 2016 to 2030 across built-up area, population, building material, earthquake risk, and multi-hazard human displacement.

4. Results and Discussion

4.1. Annual Development Profiles

4.1.1. Population and Building Exposure

Figure 9 shows local upward urbanization patterns by classifying 142 barangays in six districts into five tiers of annual growth in population and built-up floor area. Among all districts, **District 2** recorded the highest annual growth in built-up area at +2.12% (+180,308 m^2), followed by **District 5** at +1.81% (+234,479 m^2), although **District 5** has the larger annual increase in population at +1.07% (+6,254) than that of **District 2**. The results also show that, despite the lower growths, the remaining **District**

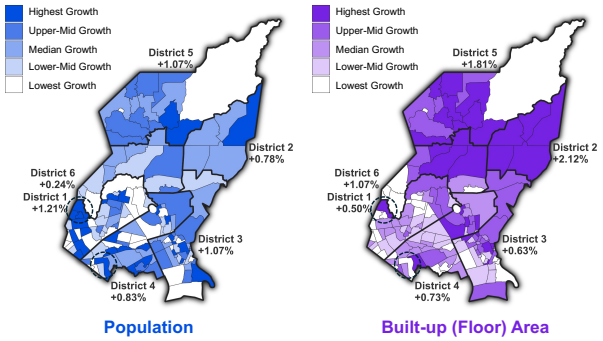

Figure 9: Annual development profile of population count (*left*) and building exposure (in terms of total built-up floor area) (*right*). The percentages are CAGR, and the numbers inside the parentheses are the average annual increase at the district level. The encircled areas are **Brgy. Balingasa** in **District 1** and **Brgy. Doña Imelda** in **District 4**.

1, **District 3**, **District 4**, and **District 6** exhibit a more spatially sparse trend in built-up area, alongside localized growth in population, particularly noticeable in **District 1** at +1.21% (+5,219). This shows that the intra-city neighborhood-level development has two distinct parts, wherein the northern portion exhibits a more balanced upward growth for both increasing built-up area for growing population, and the southern portion implies a localized densification constrained by the slower growth in built-up area. Our findings further confirm the behavioral pattern of population growth, with a preference for more developed areas, mostly located in the southern portion, that connect to neighboring urbanized cities in the Greater Metro Manila Area.

Examining further this observed localized densification in **District 1**, only one barangay, **Brgy. Balingasa**, belongs to the **Highest Growth** tier of built-up area, while 12 and 11 barangays are part of the **Lowest Growth** and **Median Growth** tiers. Despite that, in the same district, the population trends in 11 barangays are classified as **Highest Growth**, including **Brgy. Balingasa** in the **Upper-Mid Growth** tier. Another concerning case is **Brgy. Doña Imelda** in **District 4**, which recorded **Lowest Growth** in built-up area at +0.10% (+931 m^2) but overwhelmed by the **Highest Growth** in population at +5% (+1,067), notwithstanding the reported impacts in its riverine informal settlements after typhoon Ondoy in 2009 (Nunag, 2009; Saloma-Akpedonu and Lao, 2011). By understanding these trends in neighborhood-level growth in built-up areas and population, our insights into the annual development profile enable comparative analysis at the barangay level with varying growth tiers and provide evidence for prospective local management policies on the degree of urban exposure, particularly when contextualized with past disasters.

4.1.2. Building Material of Physical Vulnerability

Figure 10 presents the projected annual growth rates of four dominant construction materials, namely, **Wood**, **Masonry**, **Concrete**, and **Steel**, following our grouping in Table 1. It is important to note that these percentages are derived from approximated distributions based on housing census data, expert belief systems on building typologies, and projections inferred from spatiotemporal patterns observed in high-resolution Earth Observation data. While the resulting CAGRs do not directly measure material utilization or demand, Figure 10 provides an indication of how the composition of the building stock is expected to change over time and where future demand for specific construction materials may become concentrated. As such, these growth rates provide insights into the evolving spatial distribution of construction materials.

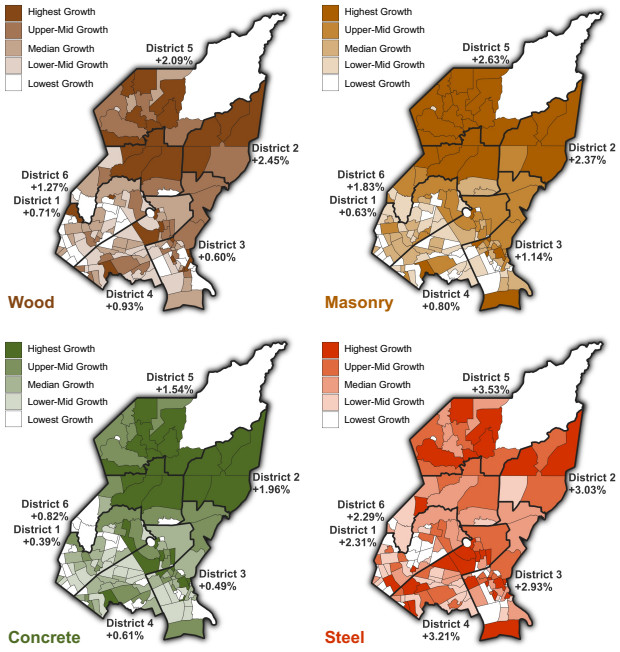

Figure 10: Annual development profile of physical vulnerability (in terms of dominant building material, see Table 1 for reference). The percentages are CAGR, and the numbers inside the parentheses are the average annual increase at the district level.

Parallel to the patterns observed for built-up area growth, the northern portion of the city, comprising **District 2**, **District 5**, and the eastern half of **District 6**, is characterized by a predominance of barangays classified under the **Upper-Mid Growth** and **Highest Growth** tiers across all construction material types. In contrast, the high-growth tiers are more sparsely distributed in the southern portion of the city, particularly in **District 1**, **District 3**, and **District 4**. This spatial pattern is consistent with the report of QCPDO (2022), which documents the northward expansion of urban development, driven by the construction of new residential subdivisions and road networks, particularly in **District 2** and **District 5**. In contrast, the same report notes that **District 1**, **District 3**, and **District 4** are already highly urbanized, with much of their remaining residential land being redeveloped into townhouses and high-rise residential

condominiums. Furthermore, the growth in **District 5** and the eastern half of **District 6** has been associated with the conversion of commercial land to residential use, while **District 2** recorded the largest conversion of commercial areas into socialized housing between 2009 and 2022 (QCPDO, 2022).

Considering that **Concrete** and **Steel** are generally more expensive than **Wood** and **Masonry** (PSA, 2026a; Arcadis, 2022), the observed material growth patterns in Figure 10 may also imply spatial differences in access to, and affordability of, construction materials across barangays. As such, the projected distributions of building materials and their spatially disaggregated estimates provide an important basis for the assessment of future physical risks, sustainability targets, and city- and barangay-level intervention programs. Such interventions may include housing affordability, construction material incentives, and post-disaster planning measures that support the estimation of potential economic losses and reconstruction costs associated with different building material types. Overall, our findings on the annual development profile of physical vulnerability demonstrate how projected changes in the composition and spatial distribution of the building stock can support local governments in promoting risk-informed urban development and long-term sustainability planning.

4.1.3. Earthquake Risk by Building Damage States

Building on the trends in building material that describes the barangay-level trajectory of physical vulnerability, Figure 11 shows how local governments can address the changes in vulnerability through housing solutions, earthquake retrofit, and recovery programs. Mapping the dynamics of expected damaged floor area under **Extensive**, **Complete**, and **Collapse** conditions can directly inform and strengthen the city's existing socialized housing and resettlement projects, Local Disaster Risk Reduction and Management Fund, and Quick Response Fund (QCPDO, 2022).

Across the city, our analyses show that **District 2** and **District 5** are characterized by barangays with **Highest Growth** under the **Complete** and **Collapse** damage states, and then **District 5** starts to increase its intra-district variability in growth tiers of their respective barangays under the less severe damage states of **Extensive**, **Moderate**, **Slight**, and **No**. To illustrate further, as the **Complete** damaged floor area in **District 2** annually increases by +2.13% (+15,965 m^2) (i.e., the highest among all districts), its top constituent barangays, **Brgy. Payatas** and **Brgy. Bagong Silangan**, also reported both about +3% (+10,815 m^2 and +15,595 m^2), respectively. These particular barangays, despite the reported largest increase in built-up floor area in Figure 9 (*right*), are also in proximity to the West Valley Fault line (see Figure 6 (*left*)) with relatively lower exposure to significant flood inundation (see Figure 6 (*right*)). This raises an important concern at the intersection of recurring hazard (i.e., flooding being more frequent than earthquakes), increasing population exposure,

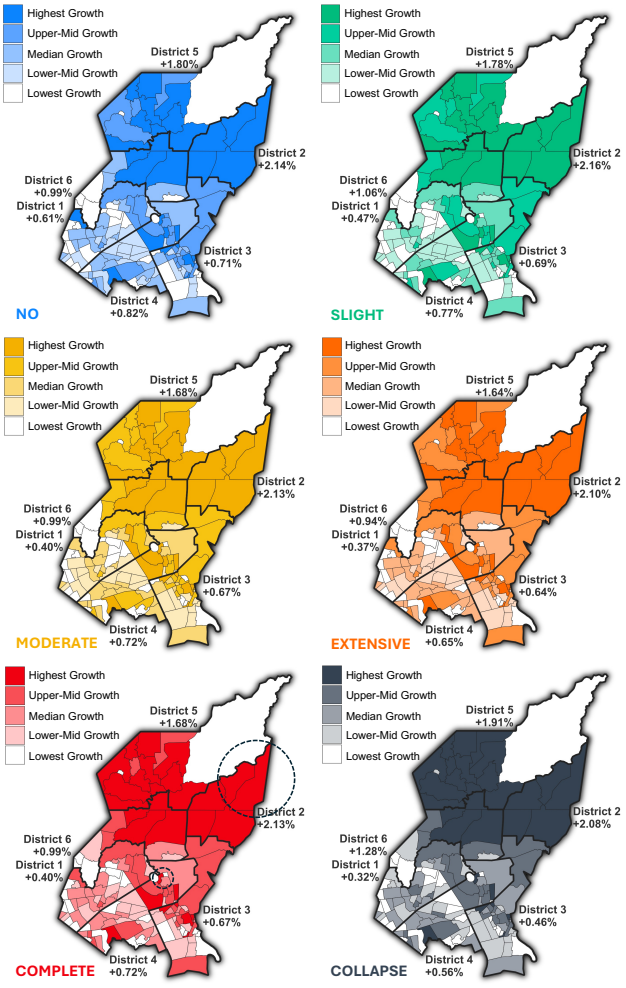

Figure 11: Annual development profile of earthquake risk (in terms of damaged floor area) by building damage state. In the bottom left, the encircled areas are the adjacent **Brgy. Payatas** and **Brgy. Bagong Silangan** in **District 2** and **Brgy. Old Capitol Site** in **District 4**.

and high physical vulnerability driven by building material affordability constraints.

However, it is also important to underscore the limitations of our trained data-driven model in predicting and projecting fine-grained material composition profiles and their subsequent earthquake risk analysis. As an example, while our results indicate that **Brgy. Old Capitol Site** in **District 4** recorded that its annual increase in **Complete** damaged floor area is in **Highest Growth** tier at +4.46% (+1,110 m^2), our investigation reveals that the trained data-driven model has a bias favoring prior distribution whose accuracy is derived from the area-based approach where a uniform compositional profile is attributed to a larger polygonal area (i.e., barangay's extent). In this case, if the prior distribution was mostly homogeneous (e.g., the majority of the built-up area is of the same building material, say **N** (makeshift or informal)), the resulting material composition of any new large-scale construction developments with unseen typology can entail a potential

Table 6
City-wide damaged floor area (EMI, 2022) and our projection, in terms of average annual increase with CAGRs in parentheses for 2016-2021, 2021-2030, and 2016-2030, respectively.

Damage State Level	EMI (2022)	2016-2030 Projection (Our Study)
No	32,901,891 m^2 (39%)	+363,170 m^2 (+1.37%, +0.84%, +1.05%)
Slight	3,362,562 m^2 (4%)	+36,109 m^2 (+1.38%, +0.81%, +1.03%)
Moderate	7,831,161 m^2 (9%)	+79,186 m^2 (+1.23%, +0.82%, +0.98%)
Extensive	11,404,898 m^2 (13%)	+107,275 m^2 (+1.10%, +0.82%, +0.92%)
Complete without Collapse	25,959,077 m^2 (31%)	+265,025 m^2 (+1.44%, +0.76%, +1.01%)
Complete with Collapse	3,250,628 m^2 (4%)	+31,649 m^2 (+1.41%, +0.72%, +0.99%)
Total	84,710,217 m^2 (100%)	+882,414 m^2 (+1.34%, +0.80%, +1.01%)

Table 7
Top ten barangays with the highest damaged floor area (m^2) in the **Complete with Collapse** damage state (EMI, 2022) and our projection, in terms of average annual increase with CAGR for 2016-2030 and its corresponding growth tier from Figure 11.

Barangays	District	EMI (2022) ↓	2016-2030 Projection (Our Study)
Batasan Hills	2	193,220 m^2	+3,002 m^2 (+1.78%) - *Highest*
Pasong Tamo	6	121,196 m^2	+1,994 m^2 (+2.18%) - *Highest*
Ugong Norte	3	110,849 m^2	+477 m^2 (+0.54%) - *Median*
Bagong Silangan	2	105,578 m^2	+1,737 m^2 (+2.81%) - *Highest*
Tandang Sora	6	102,592 m^2	+1,704 m^2 (+1.92%) - *Highest*
Holy Spirit	2	97,605 m^2	+1,349 m^2 (+1.58%) - *Highest*
Commonwealth	2	93,535 m^2	+1,885 m^2 (+2.25%) - *Highest*
Bagumbayan	3	92,111 m^2	-315 m^2 (-0.29%) - *Lowest*
Payatas	2	92,038 m^2	+1,182 m^2 (+2.91%) - *Highest*
Matandang Balara	3	91,775 m^2	+872 m^2 (+1.13%) - *Upper-Mid*

for inaccurate attribution. This is a particularly salient case where limitations can be further compounded in areas of contested development in **Brgy. Old Capitol Site** (Dovey and Recio, 2024), reflecting a transitional interface of heightened heterogeneity in building material types between the expansion of informal settlements and the reclaiming of formally developed institutional areas. This evidence not only reveals the prevailing challenges in mapping fine-grained building material typology from a methodological standpoint, but also propagates the inherent equal-sharing assumptions within a polygon vis-à-vis privacy concerns originally embedded in census data, underscoring the need for ground validation and calibration to improve building stock attribution accuracy. Whether the accuracy and applicability of our spatiotemporal results on the dynamics of vulnerability and risk are most appropriate at the building level or at the coarser barangay level should not undermine but rather acknowledge the existing poor socio-economic realities and vulnerabilities of informal settlements in **Brgy. Old Capitol Site**. These barangays are encircled with dashed lines in Figure 11 to show their relative locations on the map.

Nonetheless, our work significantly extends the CDRA (EMI, 2022) by enhancing the following key risk profiles in the city's Ecological Profile report (QCPDO, 2022). In Table 6, we present three CAGRs to separate the 2016-2021 period with higher reliability than the 2021-2030 period because of the available multi-temporal exposure observation for the former period. Our results show close CAGR values across all damage states, indicating that the current proportion and projected changes in damaged floor area are expected to remain negligible at the city level. The CAGRs for the 2021-2030 period tend to be conservatively lower than those for the earlier 2016-2021 period because of regional generalization (or smoothing) of trends, as captured by our trained data-driven model.

However, the CAGRs highly vary at the barangay level, particularly for the top ten barangays from the CDRA (EMI, 2022). Considering the **Complete with Collapse** damage state, Table 7 not only confirms our previous insights about **Brgy. Bagong Silangan** and **Brgy. Payatas** in **District 2** that are both in **Highest Growth** tier, but also supplements the existing static risk analysis with growth projections and their relative ranks in relation to local prioritization of PDRM planning. Another noteworthy case is the recorded negative CAGR for **Brgy, Bagumbayan**, which is attributable to a modeling limitation in our exposure projection. Upon closer investigation of the map, the heterogeneous urban patterns in **Brgy. Bagumbayan**, which houses the highly urbanized 'Eastwood City' with high-rise buildings alongside vulnerable informal settlements in proximity to the river and fault line, introduce non-trivial neighborhood variability to the training and generalization mechanism of the data-driven model. For example, the shadows of a high-rise building and the orientation of raw Copernicus Sentinel-2 imagery, from which the

Google Open Buildings 2.5 Temporal dataset was derived (Sirko et al., 2023), can lead to erroneous predictions of multi-temporal building heights. Hence, similar to **Brgy. Old Capitol Site**, such a complicated transitional interface with highly varying geometrical and optical characteristics has to be considered carefully for broader urban studies applying Earth observation data.

To conclude, it is important to note that the annualized earthquake risk metrics derived here and in the succeeding section are distinct from the conventional average annualized loss (AAL) in probabilistic catastrophe risk practice. While AAL integrates expected economic loss across the full probability distribution of hazard events, capturing the full volatility of large earthquake scenarios from a risk-centric standpoint, our results generated annualized growth rates of physical risk indicators conditioned on a single deterministic scenario, driven by the evolving spatiotemporal patterns of exposure and vulnerability. As such, our approach is more limited in hazard scope and temporal scale, yet uniquely positioned to the scenario-based, neighborhood-to-city context of local PDRM planning. A more direct and relevant point of comparison is the Barangay Vulnerability Index (BVI) developed by EMI (2022), which identifies hotspot barangays by integrating multiple static parameters of risk and exposure for formulating city-wide policies, as further elaborated in Section 4.2. Nevertheless, our derived annual development profiles complement and extend the static nature of BVI by capturing how physical vulnerability, exposure, and their compounding risk, as evidenced by the high variability of growth tiers across the six damage states in Figure 11, shift across barangays over time. In this way, our work not only supports the temporal extension of neighborhood-level risk prioritization for prospective DRM planning, but also provides a large-scale baseline for further calibration of derived trends against ground observations to ensure reliability in practice.

4.1.4. Earthquake Risk by Injury and Fatality

Shifting our focus from damaged floor areas, this section integrates barangay population trends with changes in built-up areas to estimate the expected annual increase in **Slight**, **Serious**, and **Life-threatening** injuries, including **Fatalities**, thereby informing the prospective design of healthcare centers and hospital beds for post-disaster first-aid response. Figure 12 shows that, among all districts, **District 1**, **District 3**, and **District 4** record a high number of barangays with **Highest Growth** across all severity levels, followed by **District 5** for most of its barangays in the **Upper-Mid Growth** tier. These are spatially consistent with the patterns of population growth in Figure 9 (*left*). Our results further support the pressing need for healthcare centers, which remains below the target ratio of 1:20,000 (QCPDO, 2022), specifically that **District 1**, **District 3**, and **District 4**, and **District 5** have shortfalls of 1, 7, 10, and 18 healthcare centers, respectively.

In the same way, Table 8 and Table 9 also enhance the CDRA of EMI (2022) with projected annual increases

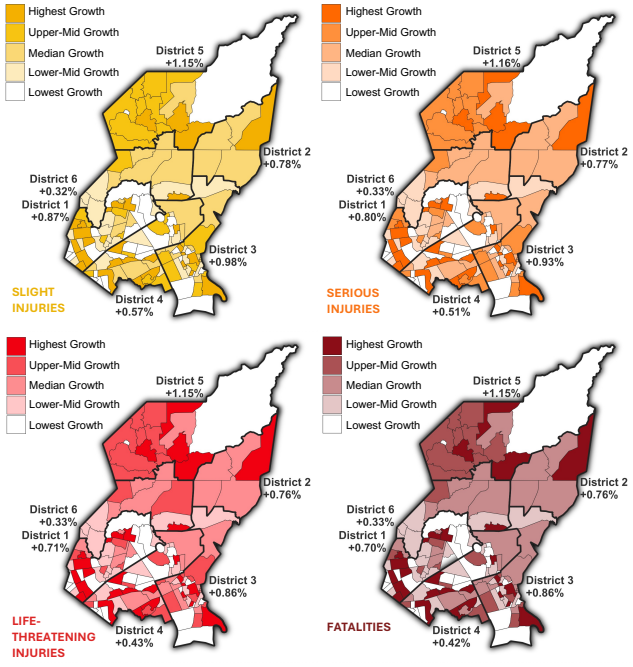

Figure 12: Annual development profile of earthquake risk in terms of casualties.

and CAGRs for casualty metrics. Our results indicate that an additional +298 beds would be necessary every year for injuries requiring hospitalization, which incrementally increases the EMI baseline estimate of 41,935. Table 8 also shows that **Life-threatening** injuries at 6,317 growing by +43 annually can be prioritized, but the number of **Serious** injuries at 35,618 growing by +255 annually can potentially overwhelm the capacity of healthcare centers. The smaller CAGRs in the 2016-2021 period relative to those in the 2021-2030 period are also consistent with the reported annual population growth rates of 0.17% (2015-2020) and 0.99% (2020-2024) from official census records (PSA, 2025). Table 9 also extends the identified top 10 barangays with annual growth rates to support local prospective design of barangay healthcare capacity, revealing that casualties in the majority of these barangays are in the **Lower-Mid Growth** and **Median Growth** tiers, except for **Brgy. Bagong Silangan**. The observed negative results for **Brgy. Culiat** and **Brgy. Matandang Balara** can be explained by the declining and slow growth of barangay population in the census years of 2015, 2020, and 2024 (PSA, 2026b). However, these results from tier comparisons do not undermine the existing risk profiles of the top ten barangays, but rather indicate an intrinsic stability in their high population and casualty proportions. Beyond these results, despite the reported satisfactory city's current capacity at 8,845 beds against the standard benchmark of about 3,000 (i.e., 1 bed is to 1,000 residents) (QCPDO, 2022), our analysis takes the scenario of an M-7.2 earthquake, which implies a sudden demand and shock to the healthcare sector. This not only reinforces the one-time importance of emergency preparedness and sustained investment in the

Table 8
City-wide injuries and fatalities (EMI, 2022) and our projection, in terms of average annual increase with CAGRs (in parenthesis) for 2016-2021, 2021-2030, and 2016-2030, respectively. The percentages in the EMI 2022 column refer to the proportion with respect to the entire city population.

Severity Level	EMI (2022)	2016-2030 Projection (Our Study)
Slight Injuries	104,955 (3.24%)	+773 (+0.43%, +0.99%, +0.77%)
Serious Injuries	35,618 (1.10%)	+255 (+0.40%, +0.96%, +0.75%)
Life-threatening Injuries	6,317 (0.19%)	+43 (+0.37%, +0.93%, +0.71%)
Injuries for Hospitalization[a]	41,935 (1.29%)	+298 (+0.40%, +0.96%, +0.74%)
Fatalities	12,494 (0.39%)	+85 (+0.36%, +0.93%, +0.71%)

[a] Injuries for Hospitalization = Serious Injuries + Life-threatening Injuries

Table 9
Top ten barangays with highest injuries and fatalities (EMI, 2022) and our projection (in parenthesis), in terms of average annual increase with CAGR for 2016-2030 and its corresponding growth tier from Figure 12.

Barangays	District	Serious Injuries	Life-threatening Injuries	Fatalities
Batasan Hills	2	3,085 (+13, +0.4%) *Median*	563 (+2, +0.5%) *Median*	1,116 (+5, +0.5%) *Median*
Commonwealth	2	2,485 (+14, +0.6%) *Median*	447 (+3, +0.6%) *Median*	885 (+5, +0.6%) *Median*
Payatas	2	1,874 (+11, +0.6%) *Median*	329 (+2, +0.6%) *Median*	649 (+4, +0.6%) *Median*
Pasong Tamo	6	1,741 (+12, +0.8%) *Median*	316 (+2, +0.8%) *Upper-Mid*	626 (+4, +0.8%) *Upper-Mid*
Bagong Silangan	2	1,714 (+37, +2.0%) *Highest*	307 (+6, +2.0%) *Highest*	607 (+13, +2.0%) *Highest*
Holy Spirit	2	1,521 (+5, +0.3%) *Median*	273 (+1, +0.3%) *Median*	541 (+2, +0.3%) *Median*
Tandang Sora	6	1,076 (+1, +0.1%) *Median*	194 (+0.2, +0.1%) *Median*	385 (+0.3, +0.1%) *Median*
Culiat	6	1,049 (-1, -0.2%) *Lower-Mid*	188 (-0.2, -0.1%) *Lower-Mid*	371 (-0.5, -0.1%) *Lower-Mid*
Matandang Balara	3	1,003 (-2, -0.2%) *Lower-Mid*	180 (-0.5, -0.3%) *Lower-Mid*	356 (-1, -0.3%) *Lower-Mid*
Bagbag	5	745 (+6, +1.3%) *Upper-Mid*	130 (+1, +1.3%) *Upper-Mid*	257 (+2, +1.2%) *Upper-Mid*

city's healthcare sector in addressing such large casualties, but also underscores that the accessibility and adequacy of healthcare capacity, spanning triage, diagnostic, and surgical services, particularly in anticipating casualties of increasing severity, will remain an urgent and recurring subject for audit and improvement.

4.1.5. Multi-Hazard Human Displacement

Human displacement due to the compounding effects of a large earthquake and extreme flooding poses a significant risk to a city's social welfare, economic resources, and long-term development (Eisner, 2014). By classifying 142 barangays into terciles (i.e., three equal groups of increasing positive CAGRs), Figure 13 illustrates how varying annual growth rates in displacement reveal the top barangays with large changes from both earthquake and flooding.

Our results show high correlation between earthquake- and flood-induced displacement growth rates, identifying the top 24 barangays (about 17% of 142) with the largest CAGRs, corresponding to 9, 5, 8, and 2 barangays in **District 1**, **District 3**, **District 4**, and **District 5**, respectively, as shown in Table 10. Figure 13 further differentiates some barangays with **HIGH** CAGR in earthquake- but **LOW** CAGR in flood-induced displacement, namely **Brgy. Lourdes** in **District 1** (+2.1%, +0.72%), and vice-versa, namely **Brgy. Krus na Ligas** in **District 4** (+0.40%, +2.7%). This evidence provides a prospective basis for assessing the relative importance of dynamic risks posed by different hazards to which these barangays are exposed.

In the histograms showing the frequency distribution of barangay CAGRs in Figure 13, the noticeable negative CAGRs (i.e, to the left part and in white color) captured the fluctuations in local barangay population from the census years of 2015, 2020, and 2024 (PSA, 2026b). This indicates that the local population shows either a degree of demographic stability and unchanging patterns or a slight decline attributable to inter-neighborhood movement. However, since the net population at the city level is growing (QCPDO, 2022), our results, which identify 45 barangays (about 32% of 142) with non-positive CAGRs across earthquake- and flood-induced human displacement, would need further examination of their underlying population dynamics. In particular, the distinction between registered barangay inhabitants and the transient population, including residents commuting from neighboring cities for employment opportunities, remains an underexplored aspect of displacement modeling at the local level.

Although EMI (2022) reported that the earthquake-induced displacement in **Brgy. Katipunan** ranks second-to-last in all 37 barangays in **District 1** with 1,031 displaced residents or about 37% of the local population, our findings reveal that its annual displacement growth from 2016 to 2030 is at +8.81% or increasing by +189 every year, due to its recent 2015-2020 densification reported in PSA (2026b). This is further compounded

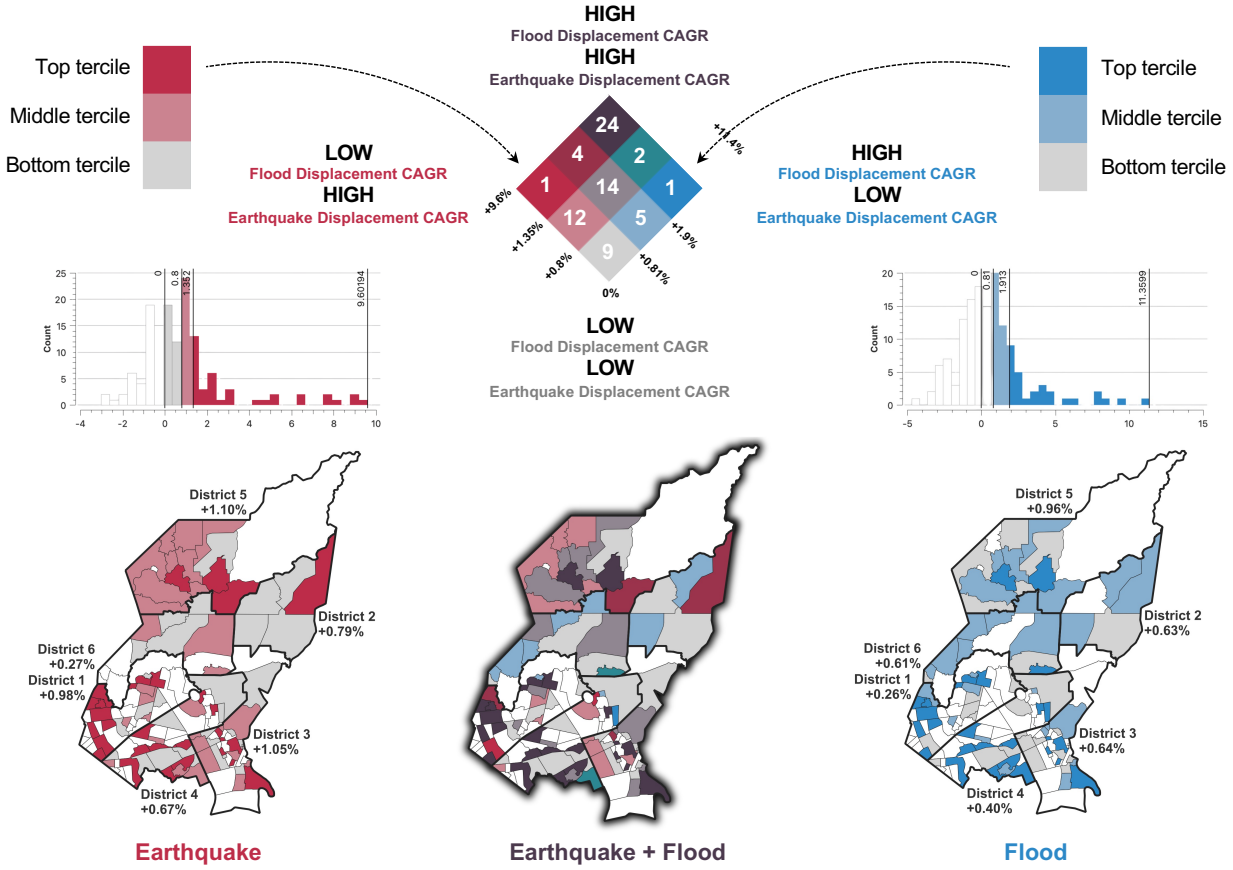

Figure 13: Annual development profile of multi-hazard human displacement under a magnitude-7.2 earthquake along the West Valley Fault in combination with a flooding simulation under the RCP8.5 with rainfall at 100-year return period. In the bivariate legend, the top 24 barangays with **HIGH** earthquake- and **HIGH** flood-induced displacement growth in terms of average annual increase and CAGR are presented in Table 10.

by the flood-induced displacement growing at +11.4% (+216) every year. Upon closer inspection, our investigation shows that this large growth is attributable to reported inconsistencies between the population census (PSA, 2026b) and the official Records of Barangay Inhabitants (BRI) (QC, 2025), which remains a contested discrepancy raised by the local government (QC, 2021). Our study, which derives the local growth rate from the available temporal data from PSA (2026b), underscores this challenge in casualty and displacement modeling at the local level in practice, in which the uncertainties in barangay population can propagate to a variety of downstream applications, such as risk-informed policymaking and social welfare prioritization programs.

Notwithstanding these concerns on local population dynamics, our work provides additional temporal insights by extending the previously known city-wide displacement metrics (EMI, 2022). Our results show that the earthquake-induced displacement of 1,561,765, or about 48% of the validated city population count of 3,242,298, is expected to grow annually by +11,670, a CAGR of +0.80%. Similarly, for the population living in one- to two-floor levels, the current estimate of flood-induced displacement of 379,734, or about 12% of the city's population, is expected to increase by +2,765, a CAGR of +0.59%. This evidence, derived from multi-temporal Earth Observation data, serves as a baseline for future work to prospectively address the demand for temporary and permanent shelters under the compounding effects of earthquakes and flooding.

4.2. Enhancing the Barangay Vulnerability Index

To support the local multi-hazard risk-informed decision-making of the city government, the EMI (2022) developed a composite index called Barangay Vulnerability Index (BVI) that identified critical barangays as a basis for local risk investment and prioritization plans. In Table 11, we append our analysis to the top 14 barangays with the highest BVI under the compounding effects of earthquake and flooding. It is important to note that these results can serve as an initial large-scale analysis, which necessitates further careful validation to contextualize the significance of the reported average annual increase and CAGRs (in parentheses).

Nevertheless, a particular case, **Brgy. Bagumbayan**, which ranks top with the highest BVI, shows contradicting results wherein its annual earthquake-damaged floor area growth falls in the **Lowest Growth** tier, in contrast to

Table 10
Top 24 barangays with **HIGH** earthquake- and **HIGH** flood-induced displacement growth in terms of average annual increase and CAGR.

		Annual Human Displacement Growth	
District	Barangay	Earthquake	Flood
1	Sta. Teresita	+613 (+9.6%)	+92 (+9.7%)
	Sto. Cristo	+709 (+8.9%)	+97 (+8.4%)
	Katipunan	+189 (+8.8%)	+216 (+11.4%)
	Kalusugan	+114 (+8.3%)	+41 (+7.9%)
	Marilag	+796 (+7.7%)	+50 (+5.7%)
	Damar	+75 (+7.7%)	+27 (+7.9%)
	Tagumpay	+117 (+6.6%)	+42 (+3.9%)
	Valencia	+420 (+6.5%)	+77 (+6.3%)
	Kaunlaran	+323 (+5.4%)	+6 (+2.9%)
3	Paligsahan	+147 (+5.2%)	+8 (+4.8%)
	Doña Imelda	+404 (+4.8%)	+326 (+4.3%)
	Bagumbayan	+599 (+4.4%)	+130 (+4.8%)
	Maharlika	+63 (+3.0%)	+52 (+2.2%)
	Sienna	+48 (+2.9%)	+38 (+2.3%)
4	Kristong Hari	+62 (+2.9%)	+34 (+3.6%)
	Manresa	+216 (+2.6%)	+111 (+2.4%)
	Pinagkaisahan	+65 (+2.4%)	+17 (+2.2%)
	Quirino 3-A	+17 (+2.3%)	+6 (+2.7%)
	Villa Maria Clara	+34 (+2.2%)	+20 (+2.0%)
	Teachers Village East	+42 (+2.0%)	+1 (+2.0%)
	Ramon Magsaysay	+110 (+1.8%)	+60 (+3.9%)
	North Fairview	+328 (+1.5%)	+120 (+2.1%)
5	Pag-ibig sa Nayon	+30 (+1.4%)	+3 (+3.7%)
	Gulod	+312 (+1.4%)	+366 (+2.1%)

its casualty and displacement metrics in the **Highest Growth** tier. This is consistent with previously observed heterogeneous urban patterns that affect the modeling of building height. Despite that, **Brgy. Bagumbayan** and its "Eastwood City" development have been extensively documented in many recent urban research as an "exceptional" and "exclusive" space (Karaan, 2016; Kleibert and Kippers, 2016; Kleibert, 2018), wherein over-densifying high-income development concentrates population growth in proximity to both hazard zones while deploying narratives of "sustainability" and "inclusive development" that exclude the low-income communities most exposed to earthquake and flood risk. **Brgy. Bagumbayan** intersects the West Valley Fault line on the western side, while it is substantially exposed to river flooding on the eastern side. This explains the sudden increase in population and the corresponding annual growth in earthquake-related casualties and multi-hazard displacement, as shown in Table 11. More recently, Ancheta et al. (2025) reported an increase in zonal values around the area, which further marginalises the urban poor in **Brgy. Bagumbayan** and surrounding neighborhoods, resulting in an increased number of informal settlements in the margins of such 'exclusive' developments (Ortega, 2014). Our findings show that, by analyzing urban patterns and their multi-hazard risk dynamics, it is imperative that equitable local development planning address the amplification of risk as a direct consequence of "exceptional" and "exclusive" spatial development.

4.3. Upgrading the Geospatial Exposure Database

Using the multi-temporal building height data both from the Google Open Buildings 2.5D Temporal dataset (Sirko et al., 2023) and our projection modeling, our work offers a potential, large-scale upgrade to the existing geospatial exposure database of EMI (2022). Figure 14 illustrates the spatial distribution of under- and over-estimated building height values across five barangays, validated against Google Street View imagery. The floor levels of mid- to high-rise buildings in **Brgy. Katipunan**, **Brgy. Kaunlaran**, and **Brgy. Balingasa** were found to be underestimated, alongside a uniform one-floor assignment to adjacent houses in **Brgy. Escopa 4** where two-floor structures are prevalent. Conversely, sparse overestimation of floor levels was identified in makeshift and informal settlements in **Brgy. Payatas**. Recognizing that the CDRA is equally reliable at the time of its implementation, given its use of the latest digital elevation and surface models and high-resolution orthoimagery, our work instead identifies strategic areas where upgrading can be prioritized to improve characterization of building attributes and enable more accurate risk assessments.

Table 11
Annual growth rates of earthquake-damaged floor area, casualties, and multi-hazard displacement across barangay vulnerability tiers, ranked by Barangay Vulnerability Index (BVI) (EMI, 2022). The numbers represent CAGRs, with corresponding tiers italicized. Note that careful validation must be in place to contextualize the significance of these growth metrics derived from Earth Observation.

					Annual Earthquake Damaged Floor Area Growth			Annual Earthquake Casualty Growth			Annual Multi-Hazard Displacement Growth	
Tier	Rank	Barangay	BVI	Dist.	Extensive	Complete	Collapse	Serious Injuries	Life-threatening Injuries	Fatalities	Earthquake	Flood
Tier 1 Very High Vulnerability	1	Bagumbayan	100	3	−0.3% *Lowest*	−0.3% *Lowest*	−0.3% *Lowest*	+4.4% *Highest*	+4.5% *Highest*	+4.5% *Highest*	+4.4% *Top*	+4.8% *Top*
	2	Claro (Quirino 3-B)	98	3	+0.9% *Upper-Mid*	+0.8% *Median*	+0.8% *Upper-Mid*	−0.5% *Lower-Mid*	−0.5% *Lower-Mid*	−0.5% *Lower-Mid*	−0.4% *Non-positive*	−0.3% *Non-positive*
	3	St. Peter	97	1	+0.4% *Median*	+0.6% *Median*	+0.5% *Median*	−0.6% *Lower-Mid*	−0.6% *Lower-Mid*	−0.6% *Lower-Mid*	−0.6% *Non-positive*	−1.6% *Non-positive*
	4	Quirino 2-B	93	3	+1.1% *Upper-Mid*	+1.2% *Upper-Mid*	+1.2% *Upper-Mid*	+1.7% *Highest*	+1.7% *Highest*	+1.7% *Highest*	+1.7% *Top*	+1.8% *Middle*
	5	Libis	92	3	+0.3% *Lower-Mid*	+0.1% *Lowest*	+0.2% *Lower-Mid*	+1.1% *Upper-Mid*	+1.1% *Upper-Mid*	+1.1% *Upper-Mid*	+1.0% *Middle*	+1.2% *Middle*
Tier 2 High Vulnerability	6	Masagana	86	3	−0.3% *Lowest*	−0.2% *Lowest*	−0.2% *Lowest*	−0.1% *Lower-Mid*	−0.1% *Lower-Mid*	−0.1% *Lower-Mid*	−0.1% *Non-positive*	−0.5% *Non-positive*
	7	Quirino 2-C	81	3	+1.8% *Highest*	+1.9% *Highest*	+1.8% *Highest*	+1.3% *Upper-Mid*	+1.3% *Upper-Mid*	+1.3% *Upper-Mid*	+1.3% *Middle*	+0.8% *Middle*
	8	East Kamias	81	3	+1.5% *Highest*	+1.5% *Highest*	+1.4% *Highest*	+0.2% *Median*	+0.2% *Median*	+0.2% *Median*	+0.3% *Bottom*	−0.3% *Non-positive*
	9	Villa Maria Clara	80	3	+0.04% *Lowest*	+0.1% *Lowest*	0.00% *Lowest*	+2.2% *Highest*	+2.1% *Highest*	+2.1% *Highest*	+2.2% *Top*	+2.0% *Top*
Tier 3 Moderate Vulnerability	10	Silangan	80	3	+0.9% *Upper-Mid*	+0.8% *Upper-Mid*	+0.7% *Upper-Mid*	+0.2% *Median*	+0.2% *Median*	+0.1% *Median*	+0.3% *Bottom*	+0.1% *Bottom*
	11	Quirino 3-A	61	3	+0.5% *Median*	+0.6% *Median*	+0.5% *Median*	+2.3% *Highest*	+2.2% *Highest*	+2.2% *Highest*	+2.3% *Top*	+2.7% *Top*
	12	Bagumbuhay	60	3	+0.7% *Median*	+0.9% *Upper-Mid*	+0.8% *Upper-Mid*	−0.1% *Lower-Mid*	−0.1% *Lower-Mid*	−0.1% *Lower-Mid*	−0.03% *Non-positive*	−0.7% *Non-positive*
	13	Mangga	57	3	+0.9% *Upper-Mid*	+0.3% *Lower-Mid*	−0.05% *Lowest*	−2.0% *Lowest*	−2.2% *Lowest*	−2.2% *Lowest*	−1.6% *Non-positive*	−4.7% *Non-positive*
	14	Quirino 2-A	55	3	+0.5% *Median*	+0.5% *Median*	+0.5% *Median*	−0.6% *Lower-Mid*	−0.6% *Lower-Mid*	−0.6% *Lower-Mid*	−0.6% *Non-positive*	−0.7% *Non-positive*

5. Conclusion and Future Work

This work examined the reliability of a geospatial database of building exposure and physical vulnerability, with particular attention to their spatiotemporal dynamics for climate and disaster risk assessment (CDRA), an increasingly central element of many prospective local government plans. Through a case study of Quezon City, Philippines, the primary aim was to demonstrate how the integration of multi-temporal Earth Observation data within a risk assessment framework advances the current state of practice in CDRA, towards a comprehensive understanding of multi-hazard urban risk dynamics across the neighborhood-to-city scale. Key findings revealed that the derived annual development profiles underscored the significance of spatiotemporal and disaggregated distributions of growth in certain building materials, damaged floor area, and casualty estimates, while enabling new directions on how these dynamics can inform a range of local policies amidst the rapidly growing urban population. The analysis further contributed to understanding the trajectories of city-wide and neighborhood-level earthquake risk metrics across varying damage states, demonstrating the viability of prospective disaster risk management under evolving exposure and vulnerability patterns. The investigation into the risk dynamics and historical development in **Brgy. Bagumbayan** provided evidence to the already well-documented challenges of equitable local development planning, where resource constraints, land availability, legal context, and housing demand collectively shape the uneven trajectories of urban risk across neighborhoods. The comparison against the existing geospatial exposure database opened an opportunity for the strategic improvement of building attribute characterization. Overall, the increasing adoption of digital mapping technologies for CDRA demands sustained scientific scrutiny and rigorous validation to support effective prospective disaster risk management at the local level. Understanding how urban risk evolves in a multi-hazard context is essential to shaping equitable long-term development plans that remain relevant to the increasing exposure of the growing vulnerable population.

This research acknowledges limitations, including propagated uncertainties arising from the limited static prior distribution of physical vulnerability and multi-temporal exposure data, particularly in highly heterogeneous urban patterns. The casualty and displacement modeling largely relied on the available multi-temporal national population data, which showed notable inconsistencies with official neighborhood-level records, a limitation that directly propagates into the multi-hazard risk estimates and

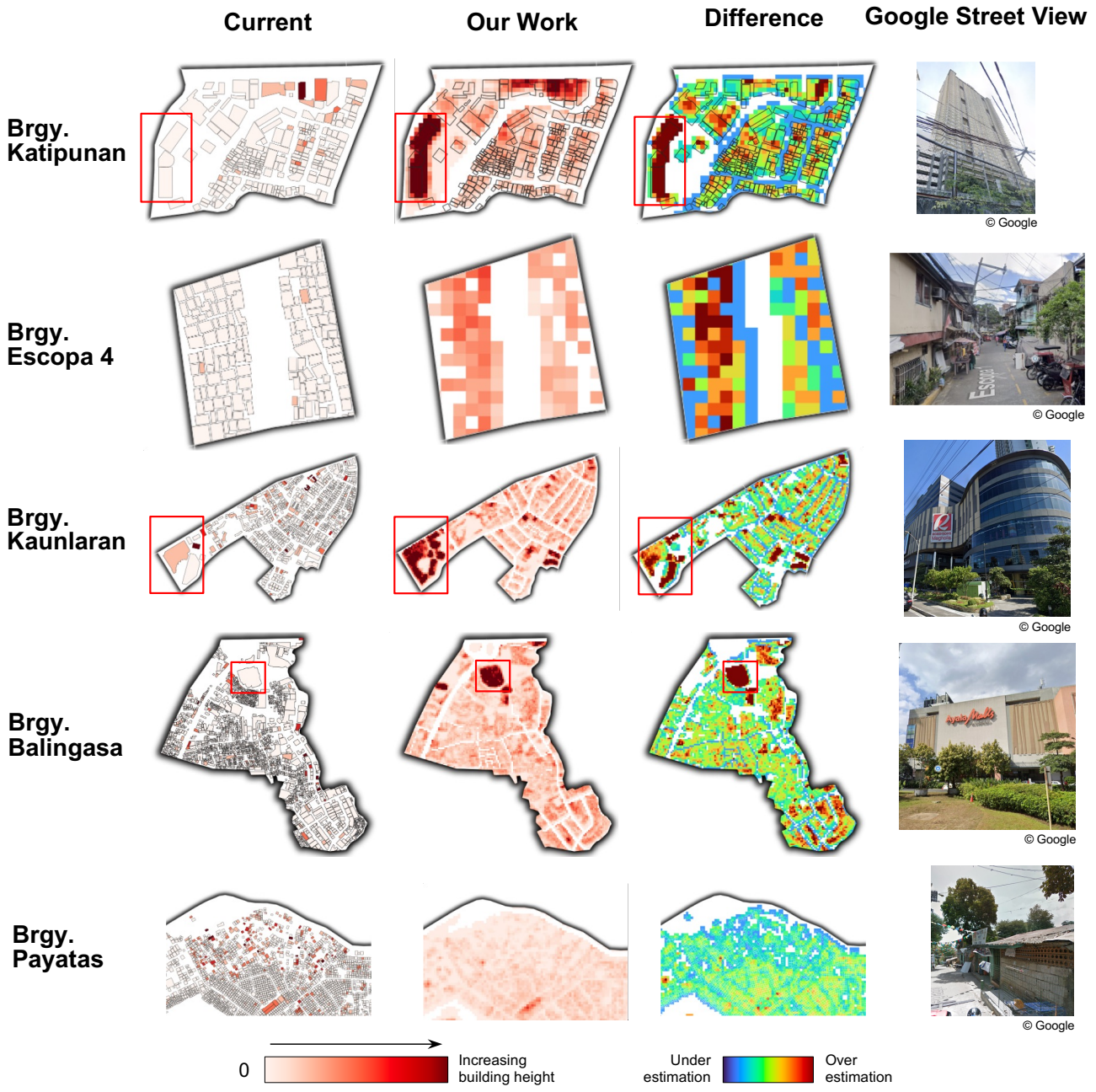

Figure 14: Five example barangays with observed noticeable difference in building heights (in increasing red color) between the CDRA (EMI, 2022) and our work. The colors in difference maps indicate underestimation (blue), overestimation (red), and negligible (green).

necessitates careful data validation prior to any operational implementation.

Future research directions should prioritize the validation of these spatiotemporal results through participatory engagement with planners, policymakers, and a broader constituency of stakeholders in Quezon City, translating the derived multi-dimensional risk profiles into representations that are more accessible and actionable for institutional practice. Such engagement could take the form of structured workshops with barangay-level planners and city disaster risk officers, map-based review sessions where stakeholders assess whether the derived risk trajectories align with their local observations, and consultative discussions that identify which risk indicators are most relevant for updating the CDRA and other downstream applications. These participatory engagement activities would ground the risk parameters in the complexities of day-to-day policymaking, and orient more targeted technical developments towards frameworks with a more direct impact on how cities manage

their exposure and risk in an inherently multifaceted governance context. Beyond participatory validation, future methodological developments may involve the integration of forward-looking machine learning approaches for urban expansion simulation (Zhu et al., 2024b,a; Geiß et al., 2024), which could complement and extend the presented probabilistic graph deep learning framework, particularly for the projection period beyond 2021 where no observed exposure data is available.

Data and Code Availability

The spatiotemporal data of building exposure and physical vulnerability, including the maps of multi-hazard risk dynamics, are publicly available at https://doi.org/10.5281/zenodo.16655873 (Dimasaka et al., 2025). The code is also accessible at https://github.com/riskaudit/GraphVSSM (Dimasaka, 2025).

Acknowledgments

This work is funded by the UKRI center for Doctoral Training in Application of Artificial Intelligence to the study of Environmental Risks (AI4ER) (EP/S022961/1). We are thankful for the building exposure and physical vulnerability data from Earthquakes and Megacities Initiative (through Urban Resilience Fellowship) (https://emi-megacities.org/) and Quezon City Disaster Risk Reduction and Management Office (through Ms. Maria Bianca Perez) (https://quezoncity.gov.ph/departments/quezon-city-disaster-and-risk-reduction-management-office/).

References

Allen, T., Ryu, H., Bautista, B., Bautista, M.L., Narag, I., Sevilla, W., Melosantos, M.L., Papiona, K., Bonita, J., 2014. Component 5 - Earthquake Risk Analysis. Enhancing Risk Analysis Capacities for Flood, Tropical Cyclone Severe Wind and Earthquake for the Greater Metro Manila Area. Philippine Institute of Volcanology and Seismology, Geoscience Australia .

Amaratunga, D., Sridarran, P., Haigh, R., Bhatia, S., Pruksapong, M.M., Panda, A., 2019. The progress of local governments in making cities resilient: state of play. Global Assessment Report on Disaster Risk Reduction (GAR 2019), United Nations Office for Disaster Risk Reduction (UNDRR) , 1–24.

Ancheta, J.A., Magno-Ballesteros, M., Ramos, T.P., 2025. Urban revitalization and shelter inadequacy: A geospatial analysis. Technical Report. PIDS Discussion Paper Series.

Arcadis, 2022. Construction Cost Handbook - Philippines 2022. Technical Report. Arcadis Philippines Inc., Makati City, Philippines.

Baker, J., Bradley, B., Stafford, P., 2021. Seismic hazard and risk analysis. Cambridge University Press.

Basu, M., Srivastava, N., Mulyasari, F., Shaw, R., 2013. Making cities and local governments ready for disasters: A critical overview of a recent approaches. Risk, Hazards & Crisis in Public Policy 4, 250–273.

Bautista, M.L., Bautista, B., Narag, I., Aquino, A., Papiona, K., Delos Santos, A.L., Nadua, J., Deximo, J.L., Jakab, M., Dunford, M., 2014. Component 2 - Exposure Information Development. Enhancing Risk Analysis Capacities for Flood, Tropical Cyclone Severe Wind and Earthquake for the Greater Metro Manila Area. Philippine Institute of Volcanology and Seismology, Geoscience Australia .

Bautista, M.L.P., Bautista, B.C., Narag, I.C., Lanuza, A.G., Deocampo, J.B., Papiona, K.L., Atando, R.A., Solidum Jr, R.U., Allen, T.I., Jakab, M., et al., 2012. Strengthening natural hazard risk assessment capacity in the Philippines. Technical Report. Geoscience Australia: Canberra.

Bennett, J., 2010. OpenStreetMap. Packt Publishing Ltd.

Cabi, N.S., Thomson, T., Gascoigne, J., Ali, H., 2021. How earth observation informs the activities of the re/insurance industry on managing flood risk, in: Earth Observation for Flood Applications. Elsevier, pp. 165–193.

Chang, S.E., Yip, J.Z., Tse, W., 2019. Effects of urban development on future multi-hazard risk: The case of vancouver, canada. Natural Hazards 98, 251–265.

Cornell, C.A., et al., 1968. Engineering seismic risk analysis. Bulletin of the Seismological Society of America 58, 1583–1606.

Costa, D.G., Bittencourt, J.C.N., Oliveira, F., Peixoto, J.P.J., Jesus, T.C., 2024. Achieving sustainable smart cities through geospatial data-driven approaches. Sustainability 16, 640.

Cremen, G., Galasso, C., McCloskey, J., 2022. A simulation-based framework for earthquake risk-informed and people-centered decision making on future urban planning. Earth's Future 10, e2021EF002388.

Cremen, G., Galasso, C., McCloskey, J., Barcena, A., Creed, M., Filippi, M.E., Gentile, R., Jenkins, L.T., Kalaycioglu, M., Mentese, E.Y., et al., 2023. A state-of-the-art decision-support environment for risk-sensitive and pro-poor urban planning and design in tomorrow's cities. International Journal of Disaster Risk Reduction 85, 103400.

Cremen, G., Gentile, R., Dabeek, J., Aljawhari, K., Manandhar, V., Rawal, P., Nocera, F., Rana, S., Zisan, B., Leandro, I., Çaktı, E., Kombe, W., 2026. Multi-hazard disaster impact analysis outputs from synthetic future urban scenarios in 10 cities.

Dimasaka, J., 2022. Towards an Equitable Development of the Regional Earthquake Resilience of the Greater Metro Manila Area, Philippines. Stanford Digital Repository, Public Policy Program. doi:doi/10.25740/kd110gb2567.

Dimasaka, J., 2025. Graph Variational State-Space Model for Probabilistic Spatiotemporal Inference of Dynamic Exposure and Vulnerability for Regional Disaster Resilience Assessment. URL: github.com/riskaudit/GraphVSSM.

Dimasaka, J., Geiß, C., So, E., 2025. A City-Scale Dataset of Annual Spatiotemporal Maps of Building Exposure and Physical Vulnerability in Quezon City, Philippines (2016–2030) via Graph Variational State-Space Model (GraphVSSM) . doi:10.5281/zenodo.16655873.

Dimasaka, J., Geiß, C., So, E., 2026a. Deepc4: Deep conditional census-constrained clustering for large-scale multitask spatial disaggregation of urban morphology. arXiv:2507.22554.

Dimasaka, J., Geiß, C., So, E., 2026b. Graphvssm: Graph variational state-space model for probabilistic spatiotemporal inference of dynamic exposure and vulnerability for regional disaster resilience assessment. Proceedings of the AAAI Conference on Artificial Intelligence 40, 38376–38384.

Dovey, K., Recio, R., 2024. Informal Settlement on UP Diliman Campus. Technical Report. UP-Center for Integrative and Development Studies.

Eisner, R., 2014. Managing the risk of compound disasters, in: Disaster risk management in Asia and the Pacific. Routledge, pp. 157–187.

EMI, 2013. Disaster Risk Reduction and Management Plan 2014-2020: Building a Disaster Resilient Quezon City Project. Technical Report. Quezon City Government and Earthquakes and Megacities Initiative.

EMI, 2022. Climate and Disaster Risk Assessment Report for Quezon City: Climate Change, Earthquake, Flood, and Landslide Hazards, including Identification of Hotspot Barangays. Technical Report. Quezon City Government and Earthquakes and Megacities Initiative.

FEMA, 2022. HAZUS Earthquake Model Technical Manual 5.1. Technical Report. Federal Emergency Management Agency, United States.

Freire, S., Aubrecht, C., Wegscheider, S., 2013. Advancing tsunami risk assessment by improving spatio-temporal population exposure and evacuation modeling. Natural hazards 68, 1311–1324.

Geiß, C., Maier, J., So, E., Schoepfer, E., Harig, S., Gómez Zapata, J.C., Zhu, Y., 2024. Anticipating a risky future: long short-term memory (lstm) models for spatiotemporal extrapolation of population data in areas prone to earthquakes and tsunamis in lima, peru. Natural Hazards and Earth System Sciences 24, 1051–1064.

Gignac-Eddy, A., Gomes, I., Ponte, E., Ghizzoni, T., Massabó, M., Mochizuki, J., Mosquera Calle, D., Mouakkid Soltesova, K., Rossi, L., Rossi, L., Rudari, R., Schiano Lomoriello, R., Trasforini, E., 2020. Guidance Note on Using the Probabilistic Country Risk Profiles for Disaster Risk Management. Technical Report. CIMA Research Foundation and International Centre on Environmental Monitoring.

Glazer, T., Hacheme, G.Q., Zaytar, A., Marotti, L., Michaels, A., Tadesse, G.A., White, K., Dodhia, R., Zolli, A., Becker-Reshef, I., et al., 2025. TEMPO: Global Temporal Building Density and Height Estimation from Satellite Imagery. arXiv preprint arXiv:2511.12104 .

HLURB, 2013. CLUP Guidebook: A Guide to Comprehensive Land Use Plan Preparation (Volume 1: The Planning Process). Technical Report. Housing and Land Use Regulatory Board.

HLURB, 2015. Supplemental Guidelines on Mainstreaming Climate Change and Disaster Risks in the Comprehensive Land Use Plan). Technical Report. Housing and Land Use Regulatory Board.

Hou, Z., Zhang, J., Zhang, M., Li, G., 2023. Hospital-system functionality quantification based on supply–demand relationship under earthquake. Natural Hazards 116, 213–234.

Huber, M., Geiß, C., Ribaira, J., Schmitt, M., Taubenböck, H., 2026. Making footprints move: Temporal disaggregation of building footprint data using sentinel-2 imagery and bayesian deep learning. Remote Sensing of Environment 340, 115413.

Huyck, C.K., Hu, Z., Eguchi, M., Esquivias, G., Amyx, P., Smith, K., Jordan, C., 2022. Characterizing uncertainty of general building stock exposure data. Earthquake Spectra 38, 2008–2025.

Jang, E., Gu, S., Poole, B., 2016. Categorical reparameterization with gumbel-softmax. arXiv:1611.01144 .

JICA, MMDA, PHIVOLCS, 2004. Earthquake impact reduction study for Metropolitan Manila, Republic of the Philippines: Final report; Vol. 2. -Main report 1. Technical Report. Japan International Cooperation Agency, Pacific Consultants International, OYO International Corp., PASCO Corp.

Karaan, A.K.I., 2016. Negotiating Spaces of Exception: Metro Manila's Planned Unit Developments, the Case of Eastwood City. Ph.D. thesis. University of Sheffield, Department of Urban Studies and Planning.

Kingma, D.P., Mohamed, S., Jimenez Rezende, D., Welling, M., 2014. Semi-supervised learning with deep generative models. Adv. Neural Inf. Process. Syst. 27.

Kipf, T.N., Welling, M., 2016. Semi-supervised classification with graph convolutional networks. arXiv:1609.02907 .

Kleibert, J.M., 2018. Exclusive development (s): Special economic zones and enclave urbanism in the philippines. Critical Sociology 44, 471–485.

Kleibert, J.M., Kippers, L., 2016. Living the good life? the rise of urban mixed-use enclaves in metro manila. Urban Geography 37, 373–395.

Lagmay, A.M.A., Santiago, J.T., Mendoza, J.E., 2024. Mainstreaming climate and disaster risk assessment in the comprehensive land use plan, in: Climate Emergency in the Philippines: Impacts and Imperatives for Urgent Policy Action. Springer, pp. 311–336.

Lee, Y., Kim, J., 2026. Multi-hazard exposure prioritization with time-varying population: Integrating seismic amplification susceptibility and flood hazards in seoul. Applied Sciences .

Loos, S., Lallemant, D., Baker, J., McCaughey, J., Yun, S.H., Budhathoki, N., Khan, F., Singh, R., 2020. G-dif: A geospatial data integration framework to rapidly estimate post-earthquake damage. Earthquake Spectra 36, 1695–1718.

Malalgoda, C., Amaratunga, D., Haigh, R., 2016. Overcoming challenges faced by local governments in creating a resilient built environment in cities. Disaster Prevention and Management: An International Journal 25, 628–648.

Marconcini, M., Metz-Marconcini, A., Esch, T., Gorelick, N., 2021. Understanding current trends in global urbanisation-the world settlement footprint suite. GI_Forum 9, 33–38.

McGuire, R.K., 2001. Deterministic vs. probabilistic earthquake hazards and risks. Soil Dynamics and Earthquake Engineering 21, 377–384.

Nelson, A.R., Personius, S.F., Rimando, R.E., Punongbayan, R.S., Tungol, N., Mirabueno, H., Rasdas, A., 2000. Multiple large earthquakes in the past 1500 years on a fault in metropolitan manila, the philippines. Bulletin of the Seismological Society of America 90, 73–85.

Nunag, A., 2009. Riverine informal settlement: Barangay Doña Imelda, Quezon City. Social Dimensions of the Impact of Typhoon Ondoy on Urban Poor Communities: Site Reports. Technical Report. Institute of Philippine Culture, School of Social Sciences, Loyola Schools, Ateneo de Manila University.

Oostwegel, L.J., Schorlemmer, D., Guéguen, P., 2025. From footprints to functions: A comprehensive global and semantic building footprint dataset. Scientific Data 12, 1699.

Ortega, A.A., 2014. Mapping Manila's Mega-Urban Region. Asian Population Studies 10, 208–235.

Pesaresi, M., et al., 2024. Advances on the global human settlement layer by joint assessment of earth observation and population survey data. International Journal of Digital Earth 17, 2390454.

Pham, H.M., Yamaguchi, Y., Bui, T.Q., 2011. A case study on the relation between city planning and urban growth using remote sensing and spatial metrics. Landscape and urban planning 100, 223–230.

Pittore, M., Haas, M., Silva, V., 2020. Variable resolution probabilistic modeling of residential exposure and vulnerability for risk applications. Earthq. Spectra 36, 321–344.

Porter, K., Hu, Z., Huyck, C., Bevington, J., 2014. User guide: Field sampling strategies for estimating building inventories. GEM Foundation .

PSA, 2025. Highlights of the National Capital Region (NCR) Population 2024 Census of Population (2024 POPCEN). URL: https://psa.gov.ph/statistics/population-and-housing/node/1684077885/.

PSA, 2026a. Construction Materials Wholesale Price Index in the National Capital Region (2018=100): April 2026. URL: https://psa.gov.ph/price-indices/cmwpi.

PSA, 2026b. The population of the barangays in Quezon City by census years. URL: https://www.citypopulation.de/en/philippines/quezoncity/.

QC, 2021. QC asks PSA to correct its "impossible" 2020 census data. URL: https://quezoncity.gov.ph/qc-asks-psa-to-correct-its-impossible-2020-census-data-some-qc-barangays-supposedly-lost-50-of-population/.

QC, 2025. Barangay Katipunan. URL: https://quezoncity.gov.ph/brgy-directory/katipunan/.

QCDRRMO, UPRI-NOAH, 2022. Drainage Master Plan Flood Hazard Simulation: Climate Change Adjusted Scenario (January 2022). Technical Report. Quezon City Government, University of the Philippines, Resilience Institute, and Nationwide Operational Assessment of Hazard (NOAH) Center.

QCPDO, 2022. 2022 Quezon City Ecological Profile. Technical Report. Quezon City Planning and Development Office, Quezon City Government.

Quigley, M., Duffy, B., 2020. Effects of earthquakes on flood hazards: a case study from christchurch, new zealand. Geosciences 10, 114.

Rentschler, J., Avner, P., Marconcini, M., Su, R., Strano, E., Vousdoukas, M., Hallegatte, S., 2023. Global evidence of rapid urban growth in flood zones since 1985. Nature 622, 87–92.

Riahi, K., Rao, S., Krey, V., Cho, C., Chirkov, V., Fischer, G., Kindermann, G., Nakicenovic, N., Rafaj, P., 2011. Rcp 8.5—a scenario of comparatively high greenhouse gas emissions. Climatic change 109, 33.

Saloma-Akpedonu, C., Lao, M.E.J., 2011. The Social Impacts of Tropical Storm Ondoy and Typhoon Pepeng. The recovery of communities in Metro Manila and Luzon. Technical Report. Institute of Philippine Culture, School of Social Sciences, Loyola Schools, Ateneo de Manila University.

Schorlemmer, D., Oostwegel, L., Calliku, D., de la Mora Lobaton, P., Zadeh, T.E., Lingner, L., Rao, C., 2026. Every building on earth–the global dynamic exposure model. Preprint .

Sirko, W., Brempong, E.A., Marcos, J.T., Annkah, A., Korme, A., Hassen, M.A., Sapkota, K., Shekel, T., Diack, A., Nevo, S., et al., 2023. High-resolution building and road detection from sentinel-2. arXiv preprint:2310.11622 .

Sirko, W., Kashubin, S., Ritter, M., Annkah, A., Bouchareb, Y.S.E., Dauphin, Y., Keysers, D., Neumann, M., Cisse, M., Quinn, J., 2021. Continental-scale building detection from high resolution satellite imagery. arXiv preprint arXiv:2107.12283 .

Stalhandske, Z., de Ruiter, M.C., Chambers, J., Zimmermann, S., Colón-González, F.J., Sairam, N., Bresch, D.N., Kropf, C.M., 2025. Global assessment of population exposure to multiple climate-related hazards from 2003 to 2021: a retrospective analysis. The Lancet Planetary Health 9.

Tingatinga, E., Pacheco, B., Hernandez Jr, J., Pascua, M., Tan, L., Suiza, R., Longalong, R., Ignacio Jr, U., Germar, F., 2019. Development of seismic vulnerability curves of key building types in the philippines, in: New Zealand Society for Earthquake Engineering Annual Conference.

UNDRR, 2025a. Global Assessment Report on Disaster Risk Reduction 2025: Resilience Pays: Financing and Investing for our Future. Technical Report. United Nations Office for Disaster Risk Reduction, Geneva.

UNDRR, 2025b. UNDRR Strategic Framework 2026-2030. Technical Report. United Nations Office for Disaster Risk Reduction, Geneva.

United Nations Office for Disaster Risk Reduction (UNDRR), 2017. The Sendai Framework Terminology on Disaster Risk Reduction. "Disaster risk management". Accessed 16 April 2026.

Wang, K., Wu, X., Chen, T.H.K., Xiao, W., 2026. Mapping precipitation-triggered landslide risks in global human settlements. Applied Geography 187, 103886.

Wood, H., Neumann, F., 1931. Modified Mercalli Intensity Scale of 1931. Seismological Society of America Bulletin 21, 277–283.

Woods, D., McKeen, T., Cunningham, A., Priyatikanto, R., Tatem, A.J., Sorichetta, A., Bondarenko, M., 2025. Global gridded multi-temporal datasets to support human population distribution modelling. Gates Open Research 9, 72.

Xia, Z., Jia, N., Yuan, B., Chen, R., Mu, H., Bi, M., Chigbu, E., Jiang, P., 2026. Long-term remote sensing reveals the development of informal settlements and their impact on land surface temperature in african drylands: A case study of windhoek, namibia. Sustainable Cities and Society , 107119.

Zhu, Y., Geiß, C., So, E., 2024a. Simulating urban expansion with interpretable cycle recurrent neural networks. GIScience & Remote Sensing 61, 2363576.

Zhu, Y., Geiß, C., So, E., Bardhan, R., Taubenböck, H., Jin, Y., 2024b. Urban expansion simulation with an explainable ensemble deep learning framework. Heliyon 10.